2016•2017
FACULTEIT GENEESKUNDE EN LEVENSWETENSCHAPPEN
master in de biomedische wetenschappen

Masterproef

High molecular weight Advanced Glycated End Products cause reduced and slower cell shortening by decreasing I_{CaL}

Promotor :
Prof. dr. Virginie BITO

Lize Evens

Scriptie ingediend tot het behalen van de graad van master in de biomedische wetenschappen

2016•2017
FACULTEIT GENEESKUNDE EN LEVENSWETENSCHAPPEN
master in de biomedische wetenschappen

Masterproef

High molecular weight Advanced Glycated End Products cause reduced and slower cell shortening by decreasing I_{CaL}

Promotor :
Prof. dr. Virginie BITO

Lize Evens
Scriptie ingediend tot het behalen van de graad van master in de biomedische wetenschappen

universiteit hasselt | Maastricht University

Acknowledgements

Starting from October until June, I conducted my senior internship at the Biomedical Research Institute at Diepenbeek. I performed experiments in the physiology-cardiology group. Without the help of several people, I could not have achieved this thesis.

First I would like to express my appreciations to my promotor professor dr. V. Bito, for the chance to conduct my senior internship in the cardiology group. Thank you for all the opportunities you gave me during this year, always supporting and helping me. Her passion and knowledge encouraged me to further explore scientific research about cardiology. Without her supervision, criticism and confidence, it was never possible to accomplish this thesis.

Second, I would like to thank my daily supervisor Dorien Deluyker. She practically taught me everything in my early 'scientific career', from bachelors till masters. Dorien let me cooperate in her experiments and writing her review. Because of her teaching qualities, she was always there for scientific questions and improvements. In this way, I could not have learned more this year and became an individual scientist. I also enjoyed the non-scientific conversations and daily talks we had. Because of this, I always felt incorporated in this research group!

Virginie and Dorien, you showed me how to work hard and become a scientist. I could not wish for better supervisors! Both of you are my scientific example of what I want to achieve in my later career!

Next I want to thank Maxim Verboven for all the help during my internship, especially during the echocardiographic measurements and analysis. Also, many thanks to all the other members of the physiology group. I always felt welcomed and integrated!

Thereafter, I would like to thank my second examiner professor dr. D. Hansen for his advice, criticism and suggestions during this project.

Finally, I would also like to thank my fellow students. Over these last eight months we have shared many stories and lunches together. Finally, I would like to thank my family and friends for the continuous support and motivation throughout the years.

Table of contents

List of abbreviations

AGEs	Advanced glycation end products
AP	Action potentials
APD	Action potential duration
AWT	Anterior wall thickness
β-AR	β-adrenergic receptors
BSA	Bovine serum albumin
BW	Body weights
CICR	Ca^{2+}-induced-Ca^{2+}-release
CML	N-carboxymethyllysine
CO	Cardiac output
CS	Citrate synthase
ECC	Excitation-contraction coupling
EDP	End-diastolic pressure
EDV	End-diastolic volume
EF	Ejection fraction
ESV	End-systolic volume
FS	Fractional shortening
HMW-AGEs	High-molecular weight AGEs
HR	Heart rate
HW	Heart weight
i.p.	Intraperitoneal
I_{CaL}	L-type Ca^{2+} current
ISO	Isoproterenol
L/L_0	Systolic cell length/diastolic cell length
LMW-AGEs	Low-molecular weight AGEs
LV	Left ventricle
LVP	Left ventricular pressure
Max dP/dt	Maximum peak time derivative
Min dP/dt	Minimum peak time derivative
NAC	N-acetyl-L-cysteine
NCX	Na^+/Ca^{2+} exchanger
NT	Normal Tyrode
PLN	Phospholamban

PLN S16	PLN phosphorylated on serine 16
PLN T17	PLN phosporylated on threonine 17
PWT	Posterior wall thickness
RAGE	Receptor for AGEs
ROS	Reactive oxygen species
RT	Room temperature
RT_{50}	Half time relaxation
SEM	Standard deviation of the mean
SERCA	SR Ca^{2+} ATPase
SR	Sarcoplasmic reticulum
sRAGE	soluble RAGE
SV	Stroke volume
τ fast	Fast time constant
τ slow	Slow time constant
TL	Tibia length
TTP	Time to peak of contraction
V_m	Resting membrane potential

Abstract

Introduction

Advanced glycated end-products (AGEs) are proteins and lipids that become glycated and oxidized after persistent contact with reducing sugars or short-chain aldehydes. There is growing evidence reporting that AGEs with a high molecular weight (HMW-AGEs) contribute to the development and progression of cardiovascular dysfunction *in vivo*. However, to date, underlying mechanisms remain elusive. In particular, effects at the cellular level remain unknown.

Material and methods

Adult male rats were daily injected intraperitoneally for 6 weeks with either HMW-AGEs (20 mg/kg/day, n=25) or a control solution (n=19). Echocardiographic and hemodynamic measurements were performed at sacrifice to assess global cardiac function. Single cardiomyocytes from the left ventricle were obtained by enzymatic dissociation through retrograde perfusion of the aorta. Unloaded cell shortening was measured during field stimulation at 1, 2 and 4 Hz and normalized to diastolic length. Time to peak of contraction and time to 50% relaxation were measured to assess kinetics of cell contraction. Finally, Ca^{2+} influx, as assessed by L-type Ca^{2+} current (I_{CaL}), was measured during whole-cell ruptured patch clamp and normalized to cell capacitance.

Results

After 6 weeks of HMW-AGEs injection, rats displayed *in vivo* cardiac dysfunction as characterized by a significant increased wall thickness and changes in peak rate pressure rise and decline. In addition, single cardiomyocytes were significantly wider. Unloaded cell shortening was significantly reduced in HMW-AGEs and was associated with slower kinetics. Finally, peak I_{CaL} density was significantly decreased in HMW-AGEs injected animals.

Discussion & conclusions

Rats subjected to high circulating HMW-AGEs display *in vitro* as well *as in vivo* structural and functional remodeling. Altogether, our data indicate that HMW-AGEs, an important component in our western diet, induce cardiac dysfunction not only observed at the organ level but also related to altered excitation-contraction coupling at the cellular level.

Samenvatting

Inleiding

'Advanced glycated end-products' (AGEs) of vergevorderde versuikerde eindproducten zijn proteïnen en vetten die versuikerd en geoxideerd worden na aanhoudend contact met reducerende suikers of korte-keten aldehydes. Steeds meer onderzoek toont aan dat AGEs met een hoog moleculair gewicht (HMW-AGEs) bijdragen aan de ontwikkeling en progressie van cardiovasculaire dysfunctie *in vivo*. Echter zijn de onderliggende cellulaire mechanismen die verantwoordelijk zijn voor deze dysfunctie nog steeds niet onderzocht.

Materiaal en methoden

Mannelijke volwassen ratten werden 6 weken lang dagelijks intraperitoneaal geïnjecteerd met HMW-AGEs (20 mg/kg/dag, n=25) of een controle oplossing (n=19). Om de globale cardiale functie te bepalen, werden bij opoffering echocardiografische en hemodynamische metingen uitgevoerd. Daarna werden individuele cardiomyocyten van het linker ventrikel geïsoleerd door middel van enzymatische dissociatie door retrograde perfusie van de aorta. Tijdens elektrische stimulatie op 1, 2 en 4 Hz werd cel inkrimping gemeten en genormaliseerd voor diastolische cel lengte. Om de kinetiek van de cel contractie na te gaan, werd de tijd tot maximale inkrimping en 50% relaxatie gemeten. Ten slotte werd L-type Ca^{2+} stroom (I_{CaL}) gemeten tijdens 'whole-cell ruptured patch clamp' en genormaliseerd voor cel capaciteit.

Resultaten

6 weken HMW-AGEs injecties veroorzaakte *in vivo* cardiale dysfunctie, gekarakteriseerd door significant toegenomen wanddikte en veranderingen in 'peak rate pressure rise & decline'. Daarnaast waren cardiomyocyten van HMW-AGEs dieren significant dikker maar niet langer vergeleken met cardiomyocyten van controledieren. Cel inkrimping was zowel significant verlaagd als trager in HMW-AGEs vergeleken met controles. Ten slotte was de I_{CaL} op +10 mV significant verlaagd in HMW-AGEs geïnjecteerde dieren.

Discussie & conclusie

Ratten die werden blootgesteld aan hoge levels HMW-AGEs, vertonen zowel *in vitro* als *in vivo* structurele en functionele remodelering. Onze data tonen aan dat HMW-AGEs, belangrijke componenten in ons westers dieet, cardiale dysfunctie induceren. Deze veranderingen op orgaanlevel zijn gerelateerd aan cellulaire veranderingen. Door dit proces wordt de excitatie-contractie koppeling in gezonde cardiomyocyten verstoord.

1. Introduction

1.1 Endogenous biosynthesis of advanced glycation end products

Advanced glycation end products (AGEs) can be formed when carbonyl groups of reducing sugars like glucose or short-chain aldehydes react with amino acids of proteins and lipids. They are synthetized *in vivo* via three different pathways (figure 1).

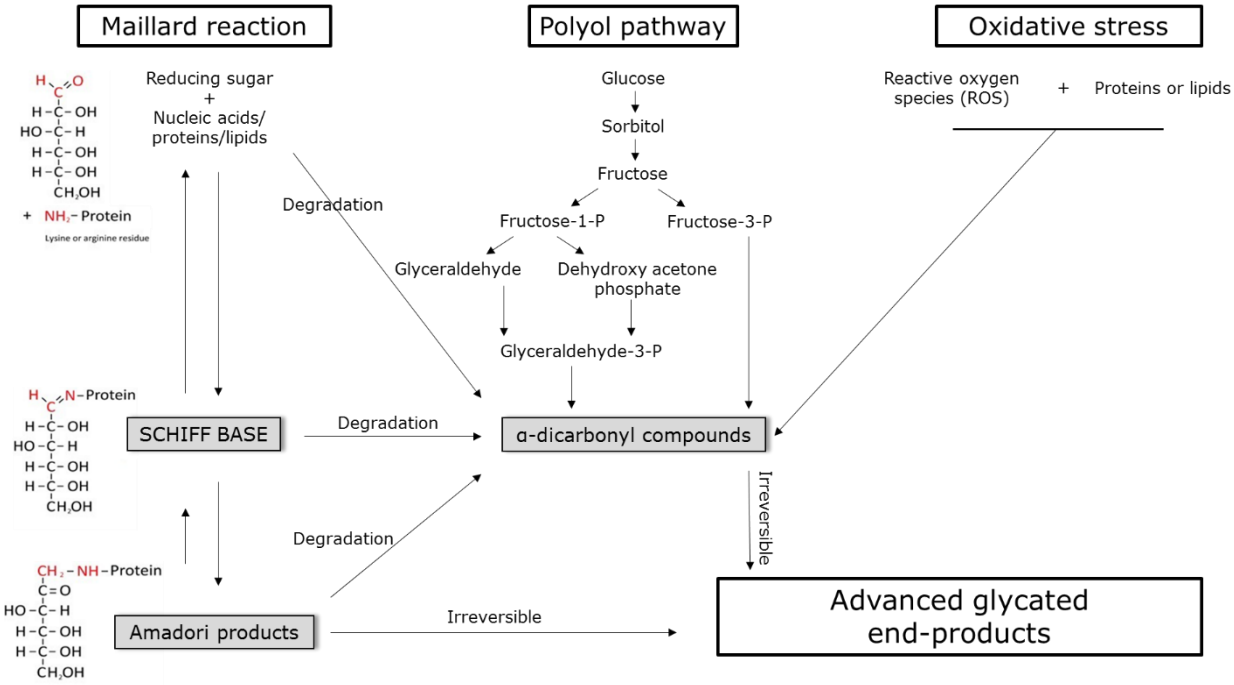

Figure 1: Formation of AGEs via Maillard, polyol and oxidative stress pathways. Figure adapted from Ott *et al.* (1)

The Maillard reaction is a reaction between glucose and amino acids of proteins, nucleic acids or lipids. In the first step of the reaction, Schiff base compounds are produced. In this step, the protein will be anchored to glucose by forming a double bound between the carbon atom of glucose and the nitrogen atom of the protein. These Schiff base compounds are unstable and rearrange to the formation of more stable so-called Amadori products. There, the hydroxyl group of the carbon moves to bond the nitrogen of the protein, resulting in a ketoamine or Amadori product. Finally, structural modifications of these products such as oxidation, dehydration or polymerization can lead to the irreversible formation of AGEs (2-4). This latest step is mainly driven by an increased reactive oxygen species (ROS) production (5). Highly reactive carbonyl groups like radicalized sugar and lipid adducts, can also be reorganized from Schiff bases or Amadori products to form α-dicarbonyl compounds (like 3-deoxyglucosone (3DG) and methylglyoxal (MGO)) (6). Metabolization of these reactive compounds can also lead to the formation of AGEs (4, 7).

The second pathway to produce AGEs *in vivo* is via the polyol pathway. This pathway results from the enzymatic formation of other components like sorbitol and fructose from glucose. Fructose can be further phosphorylated to form fructose-1-phosphate or fructose-3-phosphate. On a later stage, metabolization of these complexes can lead to the synthesis of α-dicarbonyl compounds, which are

reactive glycosylating agents. When these compounds react with monoacids, AGEs are generated irreversibly (8). As the enzymes needed in the polyol pathway use NADPH as a cofactor, other enzymes such as the glutathione reductase that also require NAPDH as cofactor, will be less activated, resulting in a reduced antioxidant defense of the cells. As a result, activation of the polyol pathway will induce both formation of AGEs and exposure of the cells to higher levels of oxidative stress (8, 9).

Finally, AGEs can also be formed in situations of increased oxidative stress, even in the absence of glucose. ROS can rapidly react with the main components of cells, like proteins or polyunsaturated fatty acids (1, 10). This process results in highly reactive products and further oxidation will lead to the formation of reactive carbonyl species (RCS) like glyoxal, methylglyoxal and malondialdehyde. By further rearrangements of these RCS, AGEs like carboxyethyllysine (CEL) or Nε-carboxymethyllysine (CML) are generated (1).

1.2 Absorption of AGEs derived from food

Independent of their endogenous formation, AGEs derived from food can be important exogenous sources. Our Western diet contains enormous levels of AGEs. Mostly food of animal origin, rich in both fat and proteins, tend to be the richest source. AGEs content also depends on the way of cooking. When food is cooked at dry and high heat, it tends to contain high concentrations of AGEs (11, 12). Normally, dietary proteins will be degraded into amino acids. However, dietary AGEs will nonetheless be absorbed by the intestines because AGEs can mask the target for proteosomal digesting. This results in around 10% absorption of dietary AGEs and later on secretion in the plasma (13), which results AGEs to circulate throughout the body. AGEs which are absorbed into the bloodstream are not totally eliminated in the urine. These AGEs can circulate and accumulate in the heart and are a major source of active toxins (14).

1.3 Mechanisms of action

There are two main mechanisms of action of AGEs (figure 2). First, they can interfere with different proteins causing cross-linking of intra-and extracellular proteins. In this way, AGEs alter their structural properties and function. Second, they can activate several receptors causing activation of signals which can lead to production of ROS or inflammatory cytokines. The best-studied AGEs receptor is the receptor for AGEs (RAGE), a member of the immunoglobulin superfamily of cell surface molecules. Activation of RAGE leads to a cascade of signaling pathways, which causes oxidative stress and hyper-responsiveness to inflammatory cytokines like TNF-α and Il-6 (11).

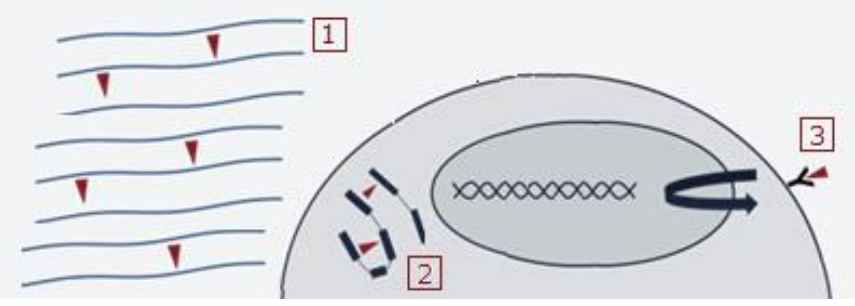

Figure 2: Mechanisms of action of AGEs. (1) AGEs can cross-link extracellular matrix proteins, (2) cross-link intracellular proteins or (3) bind receptors like RAGE.

1.3.1 Cross-linking

AGEs can form bridges between extracellular matrix proteins like collagen. Collagen has a relative long half-life varying from one to ten years. Because of this low biological turnover rate, it makes collagen susceptible for AGEs accumulation. If so, collagen fibers become linked together in an unorganized dysfunctional pattern, which is an important cause for stiffening of connective tissue (15). Vascular stiffness induces decreased vessel compliance and elevated blood pressure. In the heart, increased cross-linking can cause ventricular stiffening which results in left ventricular (LV) hypertrophy in response of pressure overload. Active relaxation or diastolic function is therefore altered (16).

AGEs can also link intracellular proteins involved in the excitation-contraction coupling (ECC). The ECC is the process from electrical excitation to contraction of the cardiomyocyte (17). In brief, electrical stimulation of the cardiomyocyte gives rise to an action potential, a transient depolarization of the membrane potential, able to trigger a transient increase in cytosolic Ca^{2+} (*i.e.* the Ca^{2+} transient) that will, ultimately, switch on the contractile machinery and initiate cell contraction. In ventricular myocytes, Ca^{2+} release from the sarcoplasmic reticulum (SR) via de ryanodine receptor (RyR) is the major source of the transient intracellular Ca^{2+} concentration rise during the excitation-contraction coupling. This release is triggered by a local increase in intracellular Ca^{2+} concentration near the Ca^{2+} release channels in the SR, the RyR (18), through a process called Ca^{2+}-induced Ca^{2+} release mechanism (CICR). CICR is considered the main mechanism involved in the ECC in ventricular myocytes. Relaxation occurs mainly through the SR Ca^{2+} ATPase (SERCA), the sarcolemmal Na^{+}/Ca^{2+} exchanger (NCX), the sarcolemmal Ca^{2+} ATPase, and the mitochondrial Ca^{2+} uniporter, the two latter pathways being less important for Ca^{2+} removal during a single beat. Overall, potential alterations of Ca^{2+} homeostasis in cardiac myocytes result in clinically significant alterations in contraction and relaxation of the whole heart (19). AGEs can cross-link the ryanodine receptor. This will result in altered cell contraction (20). Additionally, binding of AGEs to the intra-or extracellular domains of SERCA will result in partially lost activity causing prolonged and altered cardiac relaxation rates (21), resulting in both systolic and diastolic dysfunction of the heart.

1.3.2 Binding on RAGE

The interaction of AGEs with its receptor RAGE leads to the propagation of stress signals. RAGE is a transmembrane receptor localized on various cell types ranging from smooth muscle cells, neurons, hepatocytes and endothelial cells to cardiomyocytes (22). In several diseases, it is known that the expression of RAGE is up or down-regulated. For example, in Alzheimer's disease, the expression of alternative splicing isoforms of RAGE are upregulated. Data indicate that this overexpression is associated with neurodegradation (23). In multiple sclerosis, RAGE is used as a biomarker for disease progression and severity. Patients showed decreased levels of RAGE on various cell types like T-cells, monocytes and peripheral blood mononuclear cells (24). In cardiovascular disease in particular, altered RAGE expression is involved in multiple pathologies like ischemia-reperfusion or cardiac fibrosis (25). When RAGE-ligands bind their receptor, the cells respond to danger signals. Activation

of RAGE results in an inflammatory response, characterized by to the expression of several anti- and pro-inflammatory cytokines and chemokines able to modulate cardiomyocyte contractility (26).

Unlike other receptors for AGEs like AGE receptor 1 and macrophage scavenger receptor (MSR), which are involved in regulation, scavenging and degradation of AGEs, RAGE is mainly involved in signal transduction. The normal, full length RAGE is a protein which is organized into different domains. An extracellular domain (ECD), a short transmembrane domain (TMD) and an intracellular domain (ICD) (figure 3) (27). The ECD is build up out of a ligand binding site, which is a variable domain. This site is essential for receptor activation. The ECD also consist two constant immunoglobulin domains. The TMD is needed for anchoring the receptor on the membrane. The ICD is essential in transducing the signal from the cell surface to downstream pathways in the cell. Several splice variants of RAGE are known. Soluble RAGEs (sRAGE) are isoforms which are not anchored to the cell membrane. These variants lack the TMD and the ICD and are therefore circulating forms, unable to be involved in signal transduction. sRAGEs may however contribute in regulating and scavenging circulating ligands like AGEs (28). The N-terminally truncated isoform, another splice variant of RAGE, lacks the variable domain in the ECD and is not capable of binding ligands. The dominant negative form of RAGE lacks the ICD. This variant is then able of binding ligands but transducing the signal intracellular is not possible (29).

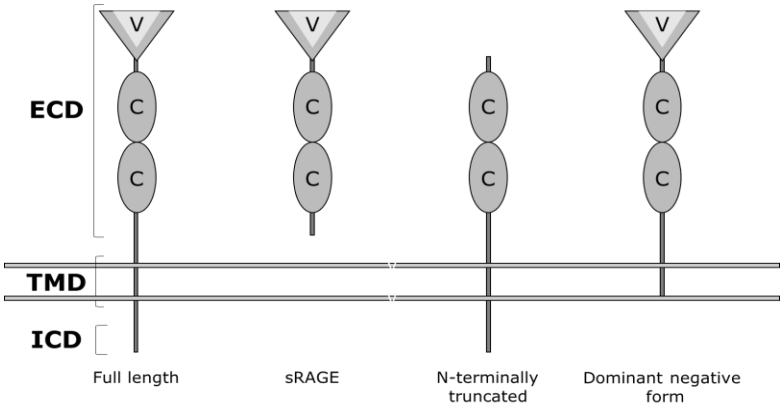

Figure 3: Different isoforms of RAGE. Full length RAGE, soluble RAGE (sRAGE), N-terminally truncated RAGE and dominant negative form RAGE. ECD = extracellular domain, TMD = transmembrane domain, ICD = intracellular domain, V = variable domain, C = constant domain.

Depending on which cell type and the duration of the stimulus (chronic or acute stimulation), different downstream signaling pathways of RAGE are activated e.g. the PKC/PI3K/Akt, JAK/STAT and MAPK/Erk pathways (22). The first two pathways are mainly involved in the upregulation of various transcription factors such as Early growth response 1 (Egr1) and Nuclear factor kappa B (NF-κβ) (22). Egr1 is mainly involved in controlling cell structure, adhesion and motility. In addition, NF-κβ can lead to activation of downstream effectors which can induce upregulation of diverse pro-inflammatory ligands (30). This leads to increased inflammatory cytokines like TNF-α and Il-6. In addition, activation of this pathway leads to ROS production. On the other hand, it has been shown that key signaling can also occur via MAPK/Erk pathways. Phosphorylation of c-Jun N-terminal kinase (JNK), a member of the MAPK family, leads to activation of GSK3B which promotes cell death (31, 32).

1.4 Low vs High molecular weight AGEs

Based on their molecular weight, AGEs can be categorized in 2 classes: low-molecular weight AGEs (LMW-AGEs) and high-molecular weight AGEs (HMW-AGEs). There is no clear boundary between LMW-AGEs and HMW-AGEs. Gerdemann *et al.* defined LMW-AGEs as proteins with a molecular mass lower than 12 kDa (33), while HMW-AGEs are molecules with a molecular mass higher than 12 kDa (33). In general, HMW-AGEs are considered to be protein-bound molecules which can form cross-links, while LMW-AGEs tent to be free proteins or non-cross-linking.

AGEs accumulate in the body with aging, which is a normal physiological process. However, it has been shown that AGEs can also accumulate at early lifetime in pathophysiological situations. For example, many studies focus and associate LMW-AGEs (e.g. CML, pentosidine and pyraline) with diabetic complications (34). However, in our western diet, AGEs formed during heat treatment can range from LMW-AGEs to HMW-AGEs (35). In fact, LMW-AGEs represent only a small amount of the total *in vivo* formed and exogenous AGEs. The role of HMW-AGEs seems to be underestimated. Indeed, data suggest that HMW-AGEs could be even more important than the known LMW-AGEs in cardiovascular alterations, independent of other diseases like diabetes (36). The accumulation of HMW-AGEs can induce cardiac dysfunction, associated with adverse outcome and survival (37). Other data also indicate that measuring only LMW-AGEs like CML is not a reliable marker and that total AGEs content including HMW-AGEs may play a substantial role in several pathologies (38). It even appears that complex AGEs, which are of a higher molecular weight, provide the highest pathogenic potential in type 2 diabetes compared with the LMW-AGEs (39). In that context, examining only LMW-AGEs levels might not be the best marker to predict the worse outcome in pathological situations. In that context, the role of HMW-AGEs in cardiovascular diseases deserve more attention.

1.5 Aim of the study

Previous studies have shown that HMW-AGEs can contribute to cardiac dysfunction. Indeed, a recent study conducted in our lab (37) indicate that increased circulating HMW-AGEs levels is associated with increased fibrosis and cross-linking, independent of RAGE activation. In this study, Deluyker *et al.* showed that HMW-AGEs cause prominent cardiac dysfunction, characterized by wall hypertrophy, increased heart sphericity and stiffness. The effects of chronically increased HMW-AGEs at the cellular level remain to date unknown. Therefore the goal of this project was to investigate whether the altered morphology and function *in vivo* after chronic exposure to HMW-AGEs was the result of structural and functional remodeling at the cellular level.

2. Material and methods

2.1 Synthesis and characterization of AGEs

HMW-AGEs were prepared as previously described (37). Briefly, bovine serum albumin (BSA) (7 mg/ml) was incubated with glycolaldehyde dimers (90 mM; Sigma-Aldrich, Diegem, Belgium) in sterile phosphate buffered saline (PBS) (pH 7.4) for 5 days at 37°C. This solution was dialyzed against PBS, 2 times for 2 hours and overnight at 4°C (3.4 kDa cut-off) to remove unreacted glycolaldehyde. Samples were concentrated with Amicon Ultra Centrifugal Filter Units (cut-off 50 kDa; Millipore, Brussel, Belgium) and filtered (0.2 µm filter, Sarstedt, Essen, Belgium) in order to remove pathogens. A control solution was prepared by incubating only BSA (7 mg/ml) in PBS in parallel with the BSA-derived AGEs. As a positive control, a commercially available AGE sample was used (Millipore, Brussel, Belgium). The self-prepared AGE samples and the commercially available sample were validated via SDS-PAGE followed by a Coomassie blue staining, examining the protein patterns of HMW-AGEs (BSA-derived AGEs), the control solution (BSA alone) and the positive control (commercial AGE sample).

2.2 Animal model

Male Sprague Dawley rats (Charles River Laboratories, Lyon, France) of ±150 grams were used. The animal protocol was approved by the Local Ethical Committee (Ethische Commissie Dierproeven, UHasselt, Diepenbeek, Belgium). The animals were daily injected intraperitoneal (i.p.) for 6 weeks with HMW-AGEs (20 mg/kg/day) (n=25) or a control solution (BSA alone; 5,5 mg/kg/day) (n=19). Echocardiographic measurements of the heart (described in section 2.4) and blood samples in the rat tail artery were taken after 6 weeks of injection in both groups. At sacrifice, hemodynamic measurements were executed to assess cardiac pressures and global cardiac function (described in section 2.5). Finally, after 6 weeks of daily injection, animals were sacrificed with an overdose of Dolethal (150 mg/kg).

2.3 Assessment of AGEs levels

Total AGEs content in plasma samples were measured using a competitive ELISA kit (OxiSelectTM Advanced Glycation End Products (AGE) Competitive ELISA kit, Cell Biolabs, Huissen, the Netherlands). Unknown AGEs concentrations in plasma samples were measured according to the protocol provided by the manufacturer. First, an AGE conjugate was coated overnight on the ELISA plate. Then, the AGE-BSA standard and plasma samples with unknown AGE concentrations were added to the coated ELISA plate. After incubation, an anti-AGE polyclonal antibody was added followed by a HRP conjugated secondary antibody. The unknown AGE concentrations in plasma samples were determined by comparison with the predetermined AGE-BSA standard curve, using a microplate reader at 450 nm.

2.4 Conventional echocardiographic measurements

Transthoracic echocardiography was performed at 6 weeks post-injection. First, rats were anesthetized with 3% isoflurane supplemented by oxygen. Echocardiography was conducted with a Vivid i ultrasound machine (GE Vingmed Ultrasound) using a 10 MHz linear array transducer. Parasternal long axis and short axis view at mid-ventricular level were acquired at a temporal resolution of ~200 frames per second. In long axis view, left ventricular (LV) diameter was measured in end-diastole ($LVEDD_{long}$) and end-systole ($LVESD_{long}$). In midventricular short axis view, posterior (PWT) and anterior wall thickness (AWT) were measured in diastole. LV diameter was also determined end-diastolic ($LVEDD_{short}$) and end-systolic ($LVESD_{short}$). M-mode echocardiography was performed at parasternal short axis view to determine HR. End-diastolic volume (EDV) was calculated as $\pi*(LVEDD_{long} * LVEDD_{short})^2)/6$. End-systolic volume (ESV) was calculated as $\pi*(LVESD_{long} * LVESD_{short})^2)/6$. Stroke volume (SV) is defined as EDV-ESV. Cardiac output (CO) is defined as SV * HR. Ejection fraction (EF) is calculated as ((EDV-ESV)/EDV) * 100 and fractional shortening (FS) is calculated as $((LVEDD_{long} - LVESD_{long})/LVEDD_{long}) * 100$. EF and FS are expressed in %.

2.5 Hemodynamic measurements

At sacrifice, hemodynamic measurements were conducted in anesthetized rats with 3% isoflurane supplemented by oxygen. Functional cardiac parameters were measured via the right carotid artery into the LV. Left ventricular pressure (LVP) and peak time derivatives maximum dP/dt and minimum dP/dt were measured with the SPR 320 Rat Pressure Catheter (AD Instruments, Germany) during 10 minutes to ensure stability of the results. Left ventricular end diastolic pressure (LVEDP), left ventricular end systolic pressure (LVESP) and time constant of LV pressure decay during isovolumetric relaxation period (Tau) was calculated with LabChart 7 software (AD instruments, Germany).

2.6 Cardiomyocyte isolation

After 6 weeks of injection, rats were injected with heparin (1000 u/kg i.p.) and sacrificed with an overdose of Dolethal (150 mg/kg i.p.). Hearts were dissected and weighted. Single adult cardiomyocytes from the LV were obtained by enzymatic dissociation through retrograde perfusion of the aorta. The hearts were perfused with normal Tyrode (NT) (in mM, NaCl 137, KCl 5.4, $MgCl_2$ 0.5, $CaCl_2$ 1, Na-HEPES 11.8, glucose 10 and taurine 20; pH 7.35) on a Langendorff setup at 37°C. After perfusion with a Ca^{2+} free solution (in mM: NaCl 130, KCl 5.4, KH_2PO_4 1.2, $MgSO_4$ 1.2, Hepes 6, glucose 20, pH 7.2), the tissue was perfused with an enzyme solution (Ca^{2+} free solution, collagenase type II (1.5 g/l; Worthington, Lakewood, USA) and protease type XIV (0.06 g/l; Sigma, Diegem, Belgium)), followed by a low Ca^{2+} solution (Ca^{2+} free solution, 100 mM $CaCl_2$). The digested LV tissue was minced and subsequently filtered with a mesh of 300 µm. Part of the freshly isolated cells were used to assess fractional cell shortening or electrophysiology measurements. Experiments were performed at room temperature within 6 h of cell isolation. Remaining cells were frozen -80°C and used for protein expression and citrate synthase (CS) activity experiments.

2.7 Fractional cell shortening measurements

Isolated cardiomyocytes were placed into a small perfusion chamber which received NT, on the stage of an inverted microscope (Nikon Diaphot). Cardiomyocyte length and width were measured in ± 30 cells per animal. Fractional cell shortening of intact cardiomyocytes was measured with a video-edge detector (Crescent Electronics, USA). Field stimulation was done with pulses of constant voltage, above threshold, using platinum electrodes. Steady-state stimuli were applied at frequencies of 1, 2 and 4 Hz. Fractional cell shortening was presented as %, normalized to diastolic cell length (L/L_0). Time to peak of contraction (TTP, ms) and half time relaxation (RT_{50}, ms) were measured to assess kinetics of cell shortening. Fractional cell shortening was also measured before and after isoproterenol (ISO; 300 nM) or N-acetyl-L-cysteine (NAC; 5 mM) application.

2.8 Electrophysiology measurements

Global electrical properties of the cells were evaluated during current-clamp by examining action potential shape and duration. L-type Ca^{2+} current (I_{CaL}) was measured during whole-cell voltage-clamp and was normalized to cell capacitance, as a measure of cell surface. Patch pipettes (2-3 MOhm) were filled with a pipette solution containing (in mM): 120 KAsp, 20 KCl, 10 HEPES, 5 MgATP, 10 EGTA, 10 NaCl (pH 7.2). I_{CaL} was measured by a single depolarizing step of 150 ms from -70 mV to +10 mV. Current-voltage relationship of I_{CaL} was also measured during 10 mV steps ranging from -50 mV to +60 mV. Steady-state inactivation and activation were determined with a classical two-steps protocol. In brief, inactivating pre-pulses of 1s were applied from a holding potential of -80 mV to various potentials. The amplitudes of the peak inward current during the test pulse (I) were normalized to their respective maximum value (I_{max}) and were plotted as a function of the inactivating potential. Steady-state activation was calculated as the peak current minus the driving force for Ca^{2+}. The amplitudes of the channel conductance during the test pulse (G) were normalized to their respective maximum value (G_{max}) and were plotted as a function of the activating potential.

2.9 Protein expression

BCA protein kit (Thermo Fisher, Erembodegem, Belgium) was used to assess protein concentrations of LV cells of both groups. By using a 12% SDS-PAGE gell with a mini protean 3 electrophoresis system (Bio-rad Laboratories, Temse, Belgium), equal amounts of proteins were separated. Gels were transferred to a polyvinylidene fluoride (PVDF) membrane. Blocking was performed during 2 hours with 5% milk in Tris-buffered solution containing 0,1% Tween-20 (TBS-T). Membranes were incubated overnight at 4°C in the presence of specific primary antibodies (SERCA, 1/4000, mouse anti-rat IgG, Santa Cruz, sc-376235, Heidelberg, Germany; PLN, 1/1000, goat anti-rat IgG, Santa Cruz, C-21923, Heidelberg, Germany; NCX, 1/1000, rabbit anti-rat IgG, Santa Cruz, sc-32881, Heidelberg, Germany; PLN S16, 1/1000, rabbit anti-rat IgG; Badrilla, A010-12, Leeds, UK; PLN T17, 1/1000, rabbit anti-rat IgG, Badrilla, A010-12AP, Leeds, UK; CS, 1/4000, rabbit anti-rat IgG, Abcam, ab129095, Cambridge, UK). All primary antibodies were diluted in 5% milk-TBS-T. Horseradish peroxidase-conjugated secondary antibodies were used and diluted 1/2000 in 5% milk-TBS-T. Proteins were visualized with the enhanced chemiluminscence (ECL) technique using Pierce ECL Plus western Blotting Substrate (Thermo Fisher, Erembodegem, Belgium). Data were normalized to β-

actin protein expression (1/1000, mouse anti-rat IgG, Santa Cruz, sc-47778, Heidelberg, Germany). Densitometry of the protein bands was quantified via the ImageQuant TL software.

2.10 Citrate synthase activity

Protein extract samples from frozen cardiomyocytes were used to assess CS activity. CS was measured according to the manufacturer's protocol (Citrate Synthase assay kit, CS0720, Sigma-Aldrich, Diegem, Belgium). CS activity, as evaluated by absorbance value monitored at wavelengths of 412 nm at 20 seconds intervals for a period of 3 minutes was assessed by using a plate reader (FLUOstar OPTIMA Microplate Reader, BMG LABTECH, Belgium). CS activity was normalized to baseline CS activity, measured without the component OAA. Data are reported in units (µmol/ml/min).

2.11 Statistical analysis

Statistical analysis was performed with Prism (Graphpad software, USA). All data are expressed as mean ± standard error of the mean (SEM). The parametric tests which were used to compare the HMW-AGEs and control group are unpaired t-tests. Paired t-tests were used to evaluate both groups before and after application of ISO or NAC. Two-way ANOVA was also used when appropriate. A value of $P<0.05$ was considered statistically significant.

3. Results

3.1 Validation of a self-prepared HMW-AGEs sample

The protein patterns of control (CTRL, BSA alone), HMW-AGEs and a commercially available AGEs sample (used as a positive control) were characterized on a SDS-PAGE via staining with Coomassie blue (figure 4). The self-prepared HMW-AGEs sample and the positive control were characterized by a smear of proteins with a high molecular weight. It is remarkable that in our HMW-AGEs sample, most of the BSA (around 66 kDa) underwent modifications related to glycation, as no specific band was seen around 66 kDa. The intensity of the band of our self-prepared HMW-AGEs sample was comparable with the intensity of the band from the purchased sample (positive control) (figure 4).

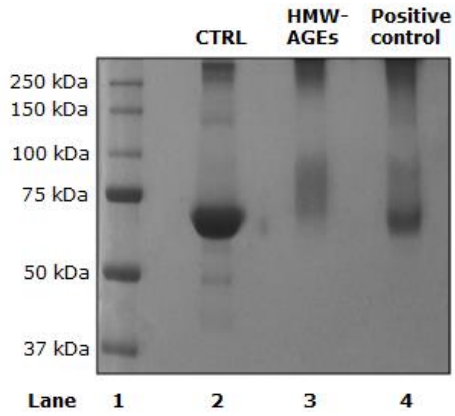

Figure 4: Characterization of HMW-AGEs samples. SDS-PAGE stained with Coomassie blue. First lane is a molecular mass marker. Second lane is control (CTRL, BSA alone) (7 mg/ml). Third lane are HMW-AGEs (BSA-derived AGEs) (7 mg/ml). Fourth lane is a positive control (commercially available AGE sample). Adapted from Deluyker *et al.* (37).

Total AGEs levels were measured in plasma samples derived from both control and HMW-AGEs animals 6 weeks post-injection. HMW-AGEs animals displayed significantly increased circulating AGEs plasma levels compared with control animals ($P<0.01$; figure 5).

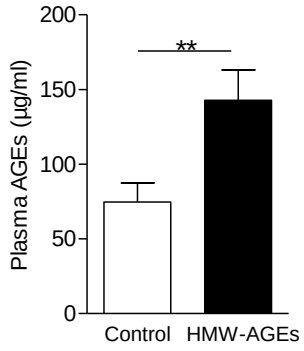

Figure 5: Total plasma AGE levels. Concentration of total AGEs in plasma samples derived from control (n=18) and HMW-AGEs (n=20) animals 6 weeks post-injection. Data are expressed as mean ± SEM. ** denotes $P<0.01$.

3.2 HMW-AGEs cause hypertrophy and alter LV function *in vivo*

Body weight (BW), heart weight (HW) and tibia length (TL) were measured at the time of sacrifice. As shown in figure 6, HW/BW and HW/TL ratios were significantly increased in HMW-AGEs animals compared with control (P<0.01).

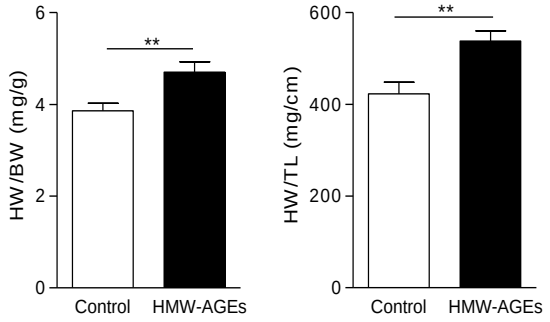

Figure 6: Effect of 6 weeks HMW-AGEs injection on heart weight. Heart weight/body weight (HW/BW; mg/g) (left) and HW/tibia length (HW/TL; mg/cm) (right) in control (n=16) and HMW-AGEs (n=17). Data are expressed as mean ± SEM. ** denotes P<0.01.

To evaluate cardiac function, conventional echocardiographic and hemodynamic measurements were performed 6 weeks post-injections. Parameters of echocardiographic measurements are summarized in table 1. HMW-AGEs injection caused significantly increased AWT (1.47 ± 0.02 mm vs 1.58 ± 0.03 mm; P<0.01) and PWT (1.56 ± 0.06 mm vs 1.77 ± 0.04 mm; P<0.01). EDV, SV, CO and EF tended to decrease, but these changes did not reach significance.

Table 1: Characteristics of echocardiographic measurements.

Parameters	6 weeks post-injections	
	Control	HMW-AGEs
HR (BPM)	360 ± 9	366 ± 9
AWT (mm)	1.47 ± 0.02	1.58 ± 0.03 **
PWT (mm)	1.56 ± 0.06	1.77 ± 0.04 **
EDV (µl)	338 ± 18	316 ± 13
ESV (µl)	82 ± 9	87 ± 6
SV (µl)	256 ± 13	229 ± 11
CO (ml/min)	92 ± 5	84 ± 4
EF (%)	76 ± 2	73 ± 2

HR, heart rate; AWT, anterior wall thickness; PWT, posterior wall thickness; EDV, end-diastolic volume; ESV, end-systolic volume; SV, stroke volume; CO, cardiac output; EF, ejection fraction. Echocardiographic measurement parameters were evaluated 6 weeks post-injections in control (n=18) and HMW-AGEs (n=25) injected animals. Data are presented as mean ± SEM. ** denotes P<0.01.

Table 2 summarizes hemodynamic parameters. As shown below, maximum dP/dt, peak rate of pressure rise used as a measure of ventricular contractility, was significantly decreased. Minimum dP/dt, peak rate of pressure decline used as a measure of ventricular relaxation, was significantly increased in the HMW-AGEs group ($P<0.05$). Other parameters such as EDP, mean pressure and Tau remained unchanged (table 2).

Table 2: Characteristics of hemodynamic measurements.

Parameters	6 weeks post-injections	
	Control	HMW-AGEs
Max pressure (mmHg)	95 ± 3	89 ± 3
EDP (mmHg)	3.6 ± 1.7	5.4 ± 2.7
Mean pressure (mmHg)	36 ± 2	37 ± 2
Max dP/dt (mmHg/s)	7356 ± 406	6283 ± 286 *
Min dP/dt (mmHg/s)	-6387 ± 266	-5426 ± 263 *
Tau (s)	0.064 ± 0.015	0.046 ± 0.015

Max pressure, maximum LV pressure; EDP, end-diastolic pressure; Max dP/dt, maximum peak time of pressure rise; Min dP/dt, minimum peak time pressure decline; Tau, time constant of LV pressure decay during isovolumetric relaxation period. LV pressure measurement parameters were evaluated 6 weeks post-injections in control (n=12) and HMW-AGEs (n=10) injected animals. Data are presented as mean ± SEM. * denotes $P<0.05$.

3.3 Cardiomyocyte morphology is altered by HMW-AGEs

Representative transmitted light images of single LV cardiomyocytes from both groups are shown in figure 7A. As shown below, mean cell width was significantly increased in HMW-AGEs (25.4 ± 0.4 µm versus 24.7 ± 0.6 µm in control, P<0.05; figure 7B left panel). In contrast, there was no significant increase in cell length (figure 7B, right panel). Data were confirmed by examining the frequency distribution of cell width and cell length. Frequency distribution of cell width was shifted rightwards in HMW-AGEs compared to control while no changes were observed in frequency distribution of cell length (figure 7C).

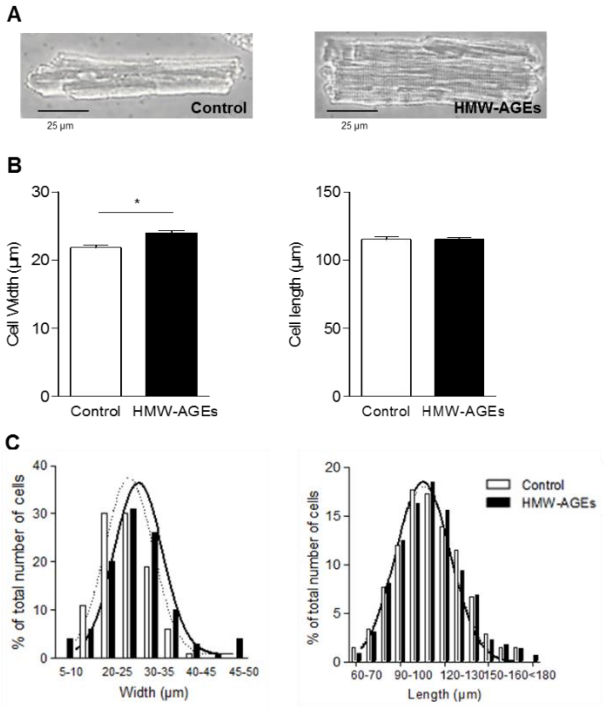

Figure 7: Morphology of isolated LV cardiomyocytes. (A) Representative transmitted light image of a single LV cardiomyocyte isolated from control (left) or HMW-AGEs (right) injected animals. (B) Analysis of cardiomyocyte width (µm) and length (µm) in control (n_{cells}= 203) and HMW-AGEs (n_{cells}= 436). (C) Frequency distribution of cardiomyocyte width and length in both groups. Data are expressed as mean ± SEM. * denotes P<0.05.

3.4 HMW-AGES cause reduced and slower unloaded cell shortening

A representative example of fractional cell shortening during field stimulation at 1 Hz in control and HMW-AGEs is shown in figure 8A. Fractional cell shortening normalized to cell length (L/L_0) at 1 Hz was significantly reduced in HMW-AGEs compared with control (figure 8B). Time to peak of contraction (TTP) and time to half-relaxation (Time to RT_{50}) at 1 Hz were both significantly increased in HMW-AGEs compared with control ($P<0.05$; figure 8B) indicating a reduced contraction associated with slower kinetics.

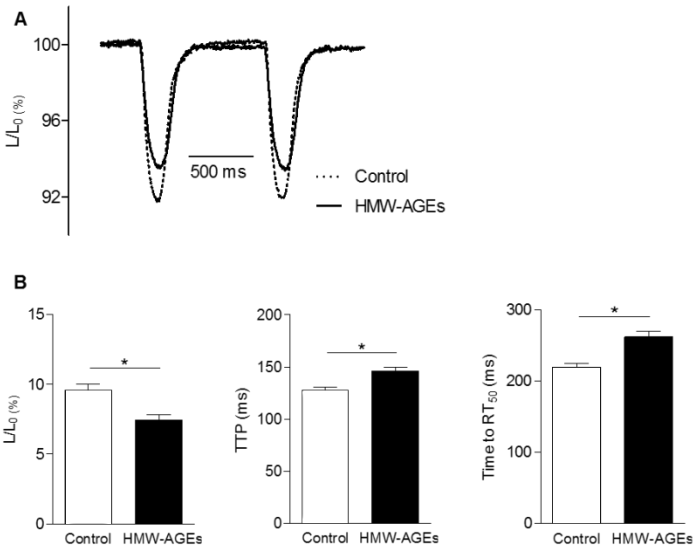

Figure 8: Cell shortening during field stimulation. (A) Representative example of fractional cell shortening during field stimulation at 1 Hz in control and HMW-AGEs cardiomyocytes. (B) Fractional cell shortening normalized to cell length (L/L_0, %) (left), time to peak of contraction (TTP, ms) (middle) and time to half-relaxation (Time to RT_{50}, ms) (right) in cardiomyocytes derived from control ($n_{cells}=64$) or HMW-AGEs ($n_{cells}=104$) injected animals. Data are expressed as mean ± SEM. *denotes $P<0.05$.

Fractional cell shortening was also significantly reduced at higher, more physiological frequencies (2 and 4 Hz) in HMW-AGEs compared with controls (figure 9). TTP and Time to RT_{50} were also significantly reduced at 2 Hz in HMW-AGEs. These differences were blunted at 4 Hz.

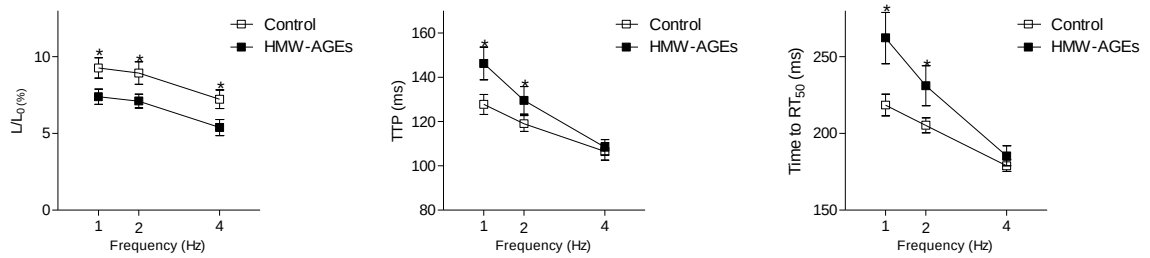

Figure 9: Frequency dependency of cell shortening during field stimulation. Frequency dependency of fractional cell shortening normalized to cell length (L/L_0, %) (left), time to peak of contraction (TTP, ms) (middle) and time to half-relaxation (Time to RT_{50}, ms) (right) at 1, 2 and 4 Hz in cardiomyocytes derived from control ($n_{cells}=64$) or HMW-AGEs ($n_{cells}=104$) animals. Data are expressed as mean ± SEM. *denotes $P<0.05$ between control and HMW-AGEs groups.

To test for a potential altered contractile reserve, unloaded cell shortening was measured before and after application of 300 nM isoproterenol (ISO), a β-agonist. As shown in figure 10A and as expected, ISO application increased fractional cell shortening at 1 Hz in control cells. The related increased shortening observed with ISO was comparable in both groups indicating an unaltered contractile reserve in HMW-AGEs treated animals. Kinetics of contraction after ISO application (i.e. TTP and Time to RT_{50}) tended to decrease in both groups (figure 10B and C).

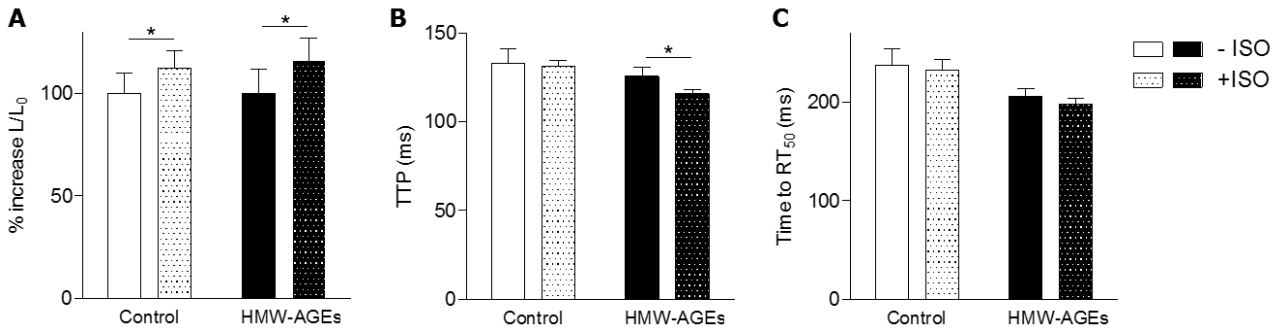

Figure 10: Effect of isoproterenol on unloaded cell shortening at 1 Hz. (A) Relative change in fractional cell shortening normalized to cell length (L/L_0, %), (B) time to peak of contraction (TTP, ms) and (C) time to half-relaxation (Time to RT_{50}, ms) at 1 Hz before and after isoproterenol (ISO) application in cardiomyocytes derived from control (n_{cells}=13) or HMW-AGEs (n_{cells}=18) injected animals. Data are expressed as mean ± SEM. – ISO = before ISO, + ISO = after ISO. * denotes $P<0.05$.

The effect of ISO on frequency dependence of unloaded cell shortening is shown in figure 11. Overall, the relative increase in fractional cell shortening after ISO was comparable in both HMW-AGEs and control cells (figure 11A). TTP and Time to RT_{50} in both groups tended to decrease after ISO application (figure 11B and C).

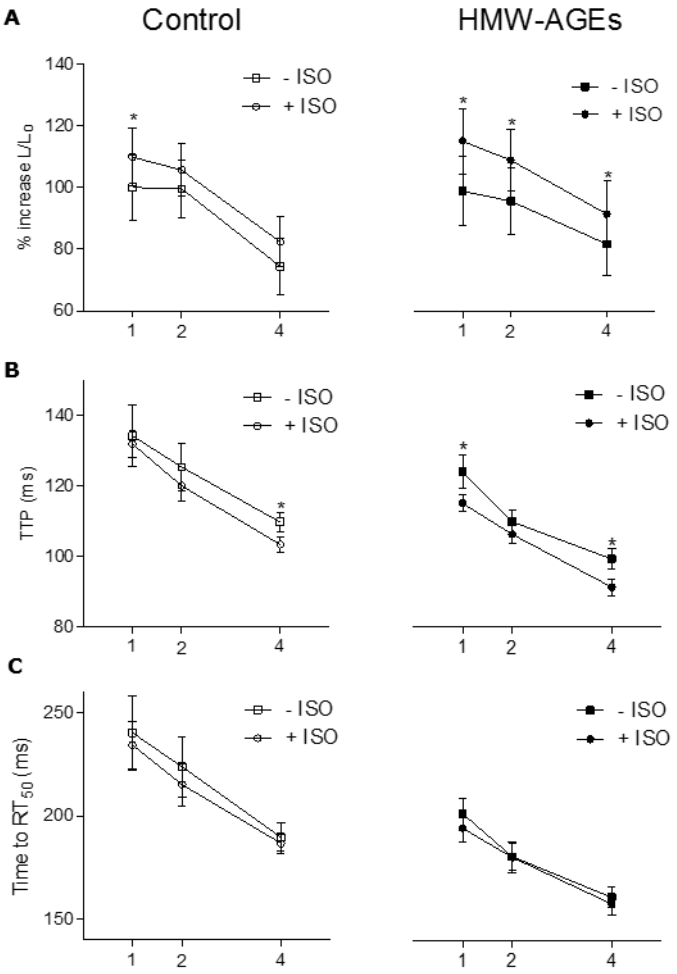

Figure 11: Effect from isoproterenol on frequency dependence of unloaded cell shortening. (A) Frequency dependence of relative change in fractional cell shortening normalized to cell length (L/L_0, %), (B) time to peak of contraction (TTP, ms) and (C) time to half-relaxation (Time to RT_{50}, ms) at 1, 2 and 4 Hz before and after isoproterenol (ISO) application in cardiomyocytes derived from control (n_{cells}=13) or HMW-AGEs (n_{cells}=18) injected animals. Left panels are control, right panels are HMW-AGEs. Data are expressed as mean ± SEM. *denotes P<0.05. - ISO = before ISO, + ISO = after ISO.

Altogether, data from figure 10 and 11 show that chronic exposure to HMW-AGEs does not alter the adrenergic response in single cells.

3.5 HMW-AGEs does not change protein expression of players involved in the excitation-contraction coupling

We further investigated whether the altered relaxation was related to changes in expression of proteins involved in ECC, namely SERCA, PLN and NCX. As shown in figure 12, no changes in protein levels of SERCA, PLN or NCX were observed between groups. Phosphorylated forms of PLN, i.e. PLN serine 16 (PLN S16) and PLN threonine 17 (PLN T17) were also not altered. The ratio SERCA/PLN, an important determinant for cell relaxation, was also not changed (data not shown).

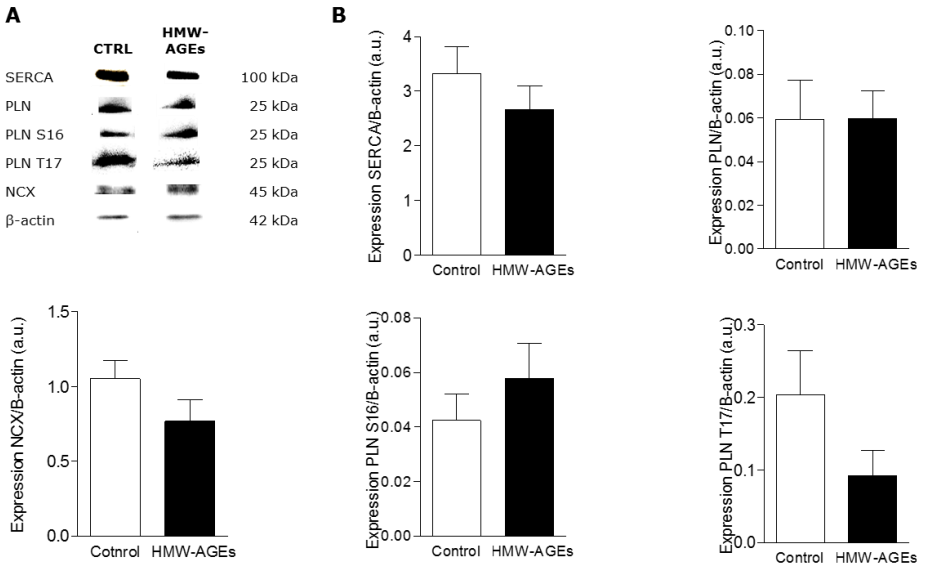

Figure 12: Expression of proteins involved in the excitation-contraction coupling. (A) Representative western blot for different excitation-contraction coupling (ECC) proteins in control (CTRL) and HMW-AGEs. (B) Quantitative analysis of different ECC proteins normalized to β-actin in control (n=7) and HMW-AGEs (n=11) injected animals. SR Ca^{2+} ATPase (SERCA), phospholamban (PLN), Na^{+}/Ca^{2+} exchanger (NCX), phosphorylated isoform of PLN on serine 16 (PLN S16) and phosphorylated isoform of PLN on threonine 17 (PLN T17). Data are expressed as mean ± SEM.

3.6 Ca^{2+} channel properties are altered by HMW-AGEs

Figure 13A is a representative example of peak L-type Ca^{2+} current (I_{CaL}) density during whole-cell voltage-clamp at a depolarizing step to +10 mV. As shown in figure 13A, peak I_{CaL} density was significantly smaller in HMW-AGEs cells compared to control. Even if the current was smaller, voltage-dependence of I_{CaL} remained bell-shaped with HMW-AGEs (figure 13C).

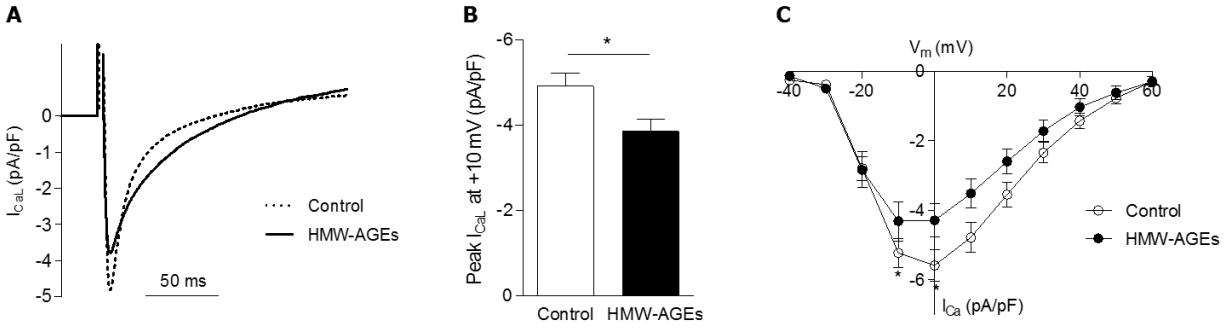

Figure 13: L-type Ca^{2+} current density. (A) Representative example of L-type Ca^{2+} current (I_{CaL}) density (pA/pF) in control and HMW-AGEs derived cardiomyocytes. (B) Peak I_{CaL} normalized to cell capacitance (pA/pF) in cardiomyocytes derived from control (n_{cells}=26) or HMW-AGEs (n_{cells}=20) injected animals. (C) Voltage-dependence of I_{CaL} in both groups. Data are expressed as mean ± SEM. *denotes P<0.05.

Figure 13A suggests a change in I_{CaL} inactivation kinetics. Ca^{2+} channel inactivation occurs by two mechanisms: voltage-dependence inactivation and Ca^{2+}-dependence inactivation. From I_{CaL} currents elicited to step to +10 mV, voltage-and Ca^{2+}-dependent inactivation were evaluated using biexponential fitting of I_{CaL} inactivation. Changes in both slow (voltage-dependent, τ_{slow}) and fast (Ca^{2+}-dependent, τ_{fast}) time constants were not statistically different. Contribution of both components in the inactivation time course was also comparable (data not shown). However, the trend to increased slow components in the HMW-AGEs group suggests a potential alteration in the intrinsic properties of the L-type Ca^{2+} channel (figure 14).

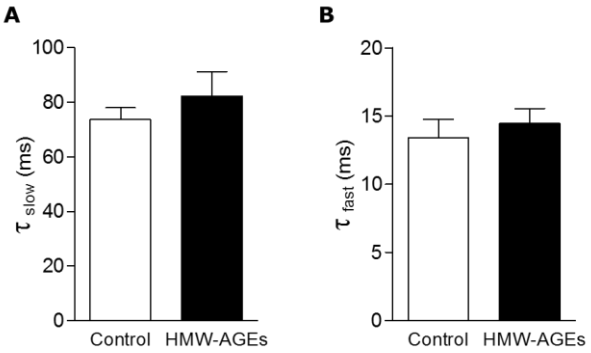

Figure 14: Kinetics of Ca^{2+}- and voltage-dependent inactivation of the L-type Ca^{2+} current. (A) slow time constant (τ_{slow}; ms), and (B) fast time constant (τ_{fast}; ms) in control (n_{cells}=21) and HMW-AGEs (n_{cells}=24) derived cardiomyocytes. Data are expressed as mean ± SEM.

To further investigate potential changes in the intrinsic properties of L-type Ca^{2+} channels, we measured steady-state inactivation and steady-state activation of I_{CaL}. As shown in figure 15A, HMW-AGEs led to a shift towards more negative potentials of steady-state inactivation of I_{CaL}, a measure of channel availability. Steady-state activation of I_{CaL}, a measure of channel conductance, also tended to be shifted towards more negative potentials, but data did not reach significance (figure 15B). These data indicate that indeed, intrinsic properties of Ca^{2+} channels are impaired in HMW-AGEs derived cardiomyocytes.

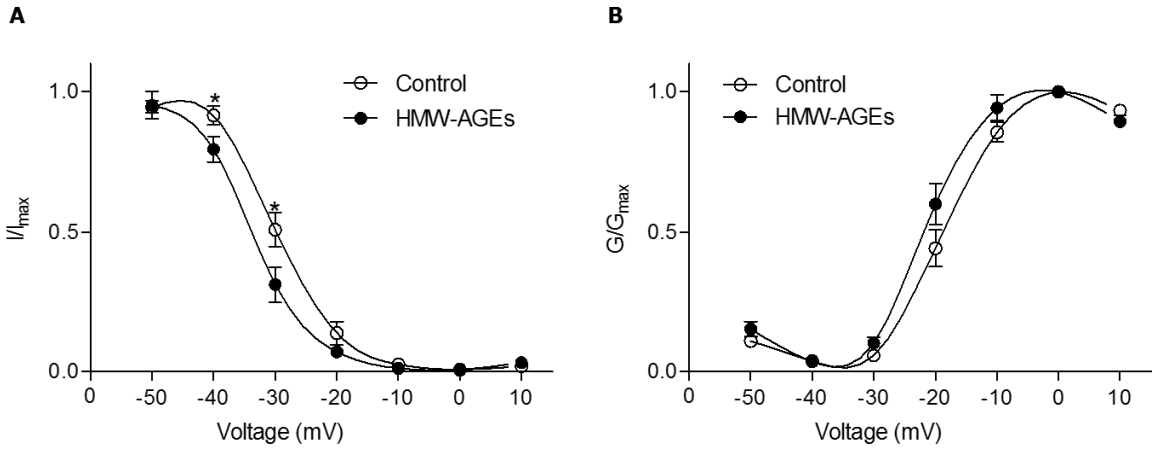

Figure 15: Steady-state inactivation and activation curves of the L-type Ca^{2+} current. (A) Steady-state inactivation of the L-type Ca^{2+} current (I_{CaL}) in control (n_{cells}=12) and HMW-AGEs (n_{cells}=8) derived cardiomyocytes. Amplitudes of the peak inward current during the test pulse (I) were normalized to their respective maximum value (I_{max}) and are plotted as a function of the inactivating potential. (B) Steady-state activation of I_{CaL} in control (n_{cells}=12) and HMW-AGEs (n_{cells}=8) derived cardiomyocytes. Amplitudes of channel conductance during the test pulse (G) were normalized to their respective maximum value (G_{max}) and are plotted as a function of the activating potential. Data are expressed as mean ± SEM. *denotes $P<0.05$.

3.7 Global cellular electrical activity is not altered by chronic exposure to HMW-AGEs

Action potential duration (APD) was measured during whole-cell current-clamp mode (figure 16). There was no difference in resting membrane potential (V_m). AP duration at 50% (APD_{50}) and at 90% (APD_{90}) repolarization tended to be increased in the HMW-AGEs group compared with the control group. Even if not reaching significance, probably due to the low number of cells, these data suggest alterations of electrical properties, implying alterations in the underlying ionic currents in HMW-AGEs.

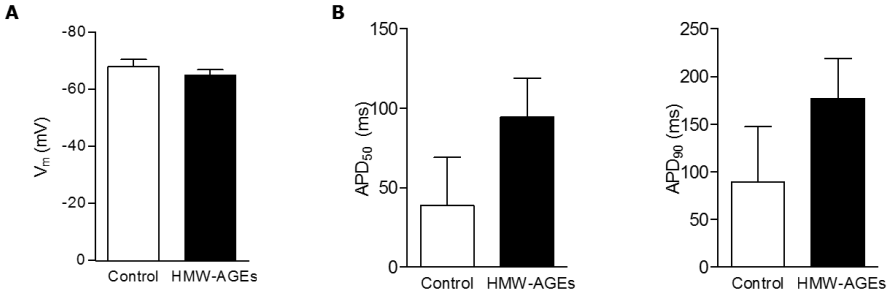

Figure 16: Action potential characteristics. (A) Resting membrane potential (V_m) and (B) action potential duration at 50% (APD_{50}) and at 90% (APD_{90}) repolarization in control (n_{cells}=5) and HMW-AGEs (n_{cells}=9) derived cardiomyocytes. Data are expressed as mean ± SEM.

3.8 Oxidative stress is not the cause for altered cellular contractile dysfunction

Alterations in mitochondrial properties could be a cause for altered ECC and contraction. As a measure for mitochondrial intactness, citrate synthase (CS) protein expression (figure 17A and B) and CS activity (figure 17C) were determined. There were no differences in CS protein expression or activity between control and HMW-AGEs samples, suggesting that HMW-AGEs did not affect mitochondria activity.

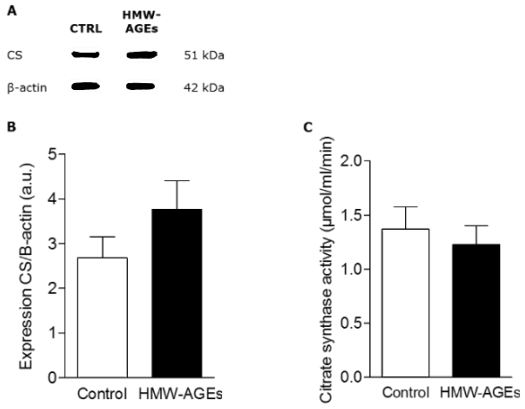

Figure 17: Protein expression of citrate synthase and citrate synthase activity. (A) Representative western blot bands for citrate synthase (CS). (B) Quantitative analysis of CS protein expression in control (CTRL; n=7) and HMW-AGEs (n=12) injected animals. (C) Quantitative analysis of citrate synthase activity in control (n=7) and HMW-AGEs (n=12) injected animals. Data are expressed as mean ± SEM.

Cardiomyocytes mitochondria are a major source of ROS. However, no changes in mitochondria activity does not necessarily mean no changes in ROS levels. Indeed, in cardiomyocytes, NADPH-dependent ROS production is also a substantial source of ROS in cardiomyocytes. To investigate whether an increase in ROS was responsible for the reduced contraction, *in vitro*, a direct ROS scavenger N-acetyl-L-cysteine (NAC, 5mM) was applied in cardiomyocytes isolated from control or HMW-AGEs injected animals. Unloaded cell shortening was measured before and after application of NAC. As summarized in figure 18, we found no difference in relative L/L_0, TTP or Time to RT_{50} between control and HMW-AGEs groups. These results suggest that that ROS is not involved in this contractile dysfunction observed in HMW-AGEs derived cardiomyocytes.

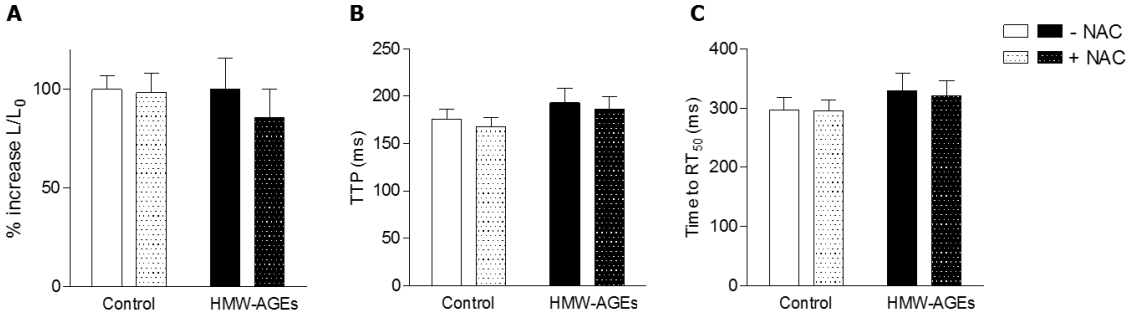

Figure 18: Effect of N-acetyl-L-cysteine (NAC) on unloaded cell shortening at 1 Hz during field stimulation. (A) Relative fractional cell shortening normalized to cell length (L/L_0, %), (B) time to peak of contraction (TTP, ms) and (C) time to half-relaxation (Time to RT_{50}, ms) at 1 Hz before and after N-acetyl-L-cysteine (NAC) application in cardiomyocytes derived from control (n_{cells}=7) or HMW-AGEs (n_{cells}=8) injected animals. Data are expressed as mean ± SEM. - NAC = before NAC, + NAC = after NAC application.

4. Discussion

In this study, we show that HMW-AGEs induce cardiac dysfunction *in vivo*, independent of other confounding factors like diabetes. These observed *in vivo* changes are related to remodeling at the cardiomyocyte level.

4.1 Increased levels of HMW-AGEs cause global cardiac dysfunction *in vivo*

First, we validated the self-prepared HMW-AGEs sample that we used in our animal model. Our data confirm that glycated products with a high molecular weight are present in our AGEs sample. To evaluate the deleterious effects of these glycated products, HMW-AGEs were daily injected in healthy rats for 6 weeks. Exogenous injection of AGEs to investigate underlying effects of these glycated products, is a widely used method. This animal model have already been used in other studies (40-42). However, this study is the first to evaluate the chronic effects of HMW-AGEs on cardiac function *in vivo* as well as *in vitro*. As expected, injection of glycated products led to an increase in total AGEs levels in the HMW-AGEs group, to the same extent as previously published (37).

As demonstrated before in our lab, HMW-AGEs cause *in vivo* dysfunction characterized by increased AWT and PWT, a typical sign of wall hypertrophy (37). Conventional echocardiographic measurements were performed to evaluate SV, CO and EF. In this study, these parameters tended to decrease but changes did not reach significance. In that context, we hypothesize that a potential decrease in SV, CO and EF could probably occur later in the disease process, but this should be further investigated in a study with a long-term follow up. Furthermore, it has to be mentioned that slight differences are hard to observe by using a 10 MHz linear array transducer but do not mean that their impact on global cardiac function is negligible. Using transducers with higher frequencies would be more accurate and would allow the detection of minor changes (43).

Corresponding to signs of hypertrophy detected by echocardiographic measurements, heart weights were also significantly increased in HMW-AGEs injected animals. Increased HW/BW and HW/TL ratios confirmed wall hypertrophy. In line with our results, other studies observed signs of hypertrophy caused by AGEs as well. A study of Candido *et al.* showed that ALT-711, an AGE cross-link breaker, is able to attenuate cardiac changes like hypertrophy (44). Another study investigated the effect of the cross-link breaker aminoguanidine (45). In that study, authors conclude that AGEs are involved in the development of hypertrophy in an animal model of heart failure with volume-overload. Comparable to our study, these studies also indicate that AGEs have an important role in the pathophysiology of heart failure.

To further assess *in vivo* function, hemodynamics were measured at sacrifice. Max and min dP/dt are parameters for the maximum rates of increase or decrease in left ventricular pressure over time (46). Max dP/dt is decreased and min dP/dt is increased by HMW-AGEs, indicating reduced ventricular contractility and relaxation induced by HMW-AGEs. As with our results, hemodynamics were also altered in a study with diabetic rats which are restored using an AGE breaker (47). Furthermore, in diabetic dogs, it has been shown that glycation end-products are a cause for hemodynamic alterations (48). In this study, treatment with AGEs breakers improves heart function, indicating a

causative role for AGEs in the pathology of diabetic cardiomyopathy. Taken together, our *in vivo* experiments show that HMW-AGEs are a cause for hypertrophy and prominent cardiac dysfunction.

4.2 HMW-AGEs have deleterious effects on cell morphology and contractile properties

Morphology of LV cardiomyocytes derived from controls and HMW-AGEs animals were examined. Mean cell width but not cell length was increased in HMW-AGEs cells, which is a sign of hypertrophy. Thickening of cardiomyocytes by AGEs has been previously described by Ko *et al*. In their study, authors demonstrate the role of glyceraldehyde-derived AGEs in H9C2 cells and their influence on cardiac hypertrophy and cell size in an acute setting (49). H9C2 cardiomyocytes show comparable responses to those observed in freshly isolated cardiomyocytes (50). However, freshly isolated adult cardiomyocytes show greater similarities in behavior and morphology *in vitro* compared with intact cardiomyocytes *in vivo* (51). In addition, mice fed with a high-fat diet were treated with an AGEs inhibitor. These mice showed reduced cell hypertrophy (52). Taken together, our study is the first to demonstrate the effects of chronic AGEs exposure on adult cardiomyocytes, without other contributing factors like high levels of fatty acids. These *in vitro* data are also in line with the hypertrophy we observe *in vivo*.

To assess the influence of HMW-AGEs on cardiomyocyte function, unloaded cell shortening during field stimulation was measured. Both at 1Hz and at higher physiological frequencies, cell shortening in HMW-AGEs cells was reduced and slower. In line with the previous *in vivo* results, contractile function in cardiomyocytes was also altered *in vitro* by HMW-AGEs. Ma *et al.* also investigated the effect of AGEs on mechanical cardiomyocyte function *in vitro* (53). In both cells derived from diabetic mice or cells acutely exposed to AGEs, peak shortening was decreased and slower compared with control cells. These alterations were counterbalanced by application of si-RNA for RAGE or an anti-RAGE antibody, suggesting that AGE-RAGE interactions are essential in the onset of cardiac diseases like diabetic cardiomyopathy. Another study of Ceylan-Isik *et al.* reported significant slower time to RT 90% in diabetic mice compared with controls (54). This defect was reversed by an AGE inhibitor. On the other hand, they found no changes in peak shortening or TTP, suggesting that AGEs do not play a major role in cardiac dysfunction, which do not confirm our results. However, the study from Ceylan-Isik *et al.* only stimulate their cells at low frequencies (< 1 Hz), which relevance is questionable as well as less physiological. Our results show that increased levels of AGEs induce cardiac alterations, independent from other diseases like diabetes. HMW-AGEs are therefore rather than being a consequence also a cause for prominent cardiac dysfunction.

Contractile reserve was investigated in our study. ISO is a full agonist to β-adrenergic receptors (β-AR) and is structurally similar to adrenaline. In normal cardiomyocytes, binding of ISO to β-AR activates a stress signal which causes increased and faster contractions. If the β-adrenergic response is altered, ISO will not have effects on contractility and contractile reserve is affected (55). However, ISO application to our cells caused significantly increased and faster cell shortening, suggesting no alterations in the contractile reserve after HMW-AGEs application. In addition, Robinet *et al.* also showed that AGEs derived from glycated albumin are not likely to block the positive chronotropic effects of another β-adrenergic agonist xamoterol (56).

4.3 ECC is altered by HMW-AGEs

To evaluate electrophysiological alterations caused by HMW-AGEs, I_{CaL} was measured during whole-cell voltage-clamp. During ECC, Ca^{2+} is transported into the cytosol via L-type Ca^{2+} channels. This Ca^{2+} influx through I_{CaL} causes Ca^{2+}-induced-Ca^{2+}-release (CICR). High levels of Ca^{2+} are transported out of the SR into the cytosol to activate myofilaments and cause activation of the ECC resulting in cardiomyocyte contraction (17). When I_{CaL} is reduced, less Ca^{2+} is transported into the cytosol, causing reduced CICR (57). In our study, I_{CaL} was significantly decreased in HMW-AGEs cells compared to controls. Kinetics of the Ca^{2+}- and voltage-dependent inactivation of I_{CaL} tended to be slower, although not reaching significance. This indicates, that besides a reduced Ca^{2+} current, Ca^{2+} influx into the cytosol is also slower. It is widely shown in various animal models of diabetes that I_{CaL} is reduced, causing altered cardiac function (58-61). Steady-state inactivation of the L-type Ca^{2+} channel, as a measure for channel availability, and steady-state activation, as a measure for channel conductance were examined during whole-cell voltage-clamp. Inactivation was significantly decreased in HMW-AGEs cells compared with control cells meaning that the L-type Ca^{2+} channel in HMW-AGEs animals is less available and inactivated more rapidly, compared to controls. Therefore, less Ca^{2+} can be transported in the cytosol and I_{CaL} is reduced. In line with our results, L-type Ca^{2+} channel inactivation is also reduced in a diabetic setting (62). Nevertheless, how AGEs have a causative role in this diabetic cardiac dysfunction is not elucidated in these studies. Therefore our study is the first to show the direct effect of HMW-AGEs on I_{CaL} and channel availability.

Next, the influence of HMW-AGEs on protein expression of important players involved in ECC were examined. In normal cardiomyocytes, SERCA pumps Ca^{2+} back into the SR to reduce the intracellular Ca^{2+} concentration, causing cardiomyocyte relaxation (17). In this way, decreased SERCA activity can cause alterations in relaxation. Reduced SERCA activity can be due to the decreased SERCA expression, although alterations in PLN function may contribute as well. PLN function is determined by its expression levels and phosphorylation status. In heart failure, PLN expression is not altered, but typically there is a reduced phosphorylation. This results in an increased function of PLN, which enhances the SERCA inhibition and, as such, reduces the SERCA activity (63-65). Generally in cardiac dysfunction, NCX activity is greater, which refers to both the NCX forward mode and the NCX reverse mode. Enhanced NCX forward mode activity causes NCX to compete better with SERCA, so that more Ca^{2+} is extruded from the cardiomyocyte and less Ca^{2+} can enter the SR (64). In contrast, the enhanced NCX reverse mode activity ensures that more Ca^{2+} can enter the cardiomyocyte during systole, thereby limiting the contractile dysfunction caused by the reduced SERCA activity (65). In our study, as expected, SERCA and PLN T17 expression tended to be reduced but changes were not significant, probably due to a low power of the study. PLN S16 and NCX protein expression tended to change by HMW-AGEs, but data did not reach significance. Total PLN protein expression was also not altered by HMW-AGEs.

In diabetic animal models, it is widely shown that SERCA expression is decreased and PLN expression is increased causing arrhythmias and diabetic cardiomyopathy (66-68). On the other hand, other studies found that there was no change in expression of PLN between diabetic and control rats (69). At the present time, there is no clear explanation for this discrepancy. In that context, a study from Petrova *et al.* investigated the effect of AGEs on SERCA, PLN and NCX protein expression. Fetal

mouse cardiomyocytes were exposed to AGEs for 24 hours. Protein expression of these players involved in ECC were not affected by AGEs (70). This is comparable to the results of our study, where both SERCA, PLN and NCX tended to be changed without however reaching significance. In our study, a possible explanation is that these minor changes might have a cumulative effect and alter ECC altogether. In addition, besides protein expression, the activity of these proteins might have a major impact on the ECC process. If HMW-AGEs cross-link these proteins, their activity might change but their expression is not altered (21). This specific aspect would require more experiments to identify whether not only protein expression but also protein activity of SERCA, PLN and NCX are altered by HMW-AGEs.

Finally, global electrical activity of the cardiomyocytes were evaluated by examining action potential (AP) shape and duration. AP were measured in control and HMW-AGEs cells. APD_{50} and APD_{90} tended to increase in HMW-AGEs cells but changes were not significant, probably due to low cell number. In an acute setting of high levels of posttranslational modified glucose application, Ren *et al.* showed a prolongation of APs (71). In addition, APD is increased in cardiomyocytes derived from diabetic rats (72). In our setting, more experiments are needed to draw firm conclusions about the effect of HMW-AGEs on APD.

4.4 Does oxidative stress contribute to cardiac dysfunction?

To evaluate how oxidative stress is involved in the cardiac dysfunction caused by HMW-AGEs, a pilot study was conducted.

In heart failure patients, it has been shown that mitochondria are the major source of ROS production (73). Indeed, changes in mitochondria structure and organisation may alter subcellular energy transfer and may contribute to altered contractile function (74). Therefore, as a measure for mitochondrial intactness, citrate synthase (CS) protein expression and activity were determined. There were no differences in CS protein expression or activity between control and HMW-AGEs samples. These data suggest that mitochondria from both groups are not dysfunctional.

Previously it has been reported that ROS alter Ca^{2+} homeostasis in cardiomyocytes, resulting in reduced contraction and altered kinetics (75). We hypothesized that increased HMW-AGEs levels induced situations of ROS imbalance, which can be responsible for the observed cardiac dysfunction. If ROS was decreased and further scavenged, cardiac function could be partially restored. Therefore, we used NAC to determine if unloaded cell shortening was improved by scavenging ROS. However, no differences in cell shortening between controls and HMW-AGEs groups were observed after NAC application, suggesting that ROS was not involved in this process. In order to draw any conclusions about the role of ROS in the contractile dysfunction and altered ECC, more specific experiments have to be performed. By reducing I_{CaL}, depleting Ca^{2+} in the SR by enhancing leakage from RyR, activating important kinases like CaMKII and PKA or affecting SERCA and NCX, ROS can alter heart function (76). Therefore, how ROS is involved in the cardiac dysfunction caused by HMW-AGES needs to be examined more in detail.

4.5 Future perspectives

Although we have demonstrated in this study that HMW-AGEs cause *in vivo* and *in vitro* cardiac dysfunction, more specific underlying mechanisms need to be investigated, e.g. evaluate Ca^{2+} handling in HMW-AGEs derived cardiomyocytes.

First, changes in SR Ca^{2+} content should be investigated in our model. Altered SR Ca^{2+} content is known to contribute to Ca^{2+} homeostasis imbalance observed in cardiomyocytes treated with HMW-AGEs. It has been widely shown in diabetes, that SR Ca^{2+} content is depleted. In this way, less Ca^{2+} can be pumped out of the SR and contraction is altered. It has already been shown that treatment with AGEs breakers restore SR Ca^{2+} depletion in diabetic rats (54, 77). These studies show an important influence of AGEs on SR Ca^{2+} content. However, to date, there is no study which examines the influence of HMW-AGEs on SR Ca^{2+} content.

Another reason for impaired cardiomyocyte functional properties could potentially be a change in myofilament sensitivity. Several studies have demonstrated that Ca^{2+} sensitivity is diminished in skinned cardiomyocytes in a diabetic setting (78-80). However, how AGEs play a role in this process, is not known. Therefore, experiments on skinned cardiomyocytes are needed and will be performed in the future to elucidate whether changes in myofilament properties are responsible for the altered cardiomyocyte contraction *in vitro* as well as *in vivo*.

In addition, the potential of ROS in cardiac dysfunction requires further attention. In particular, how ROS is involved in the cardiac dysfunction caused by HMW-AGEs is not known. Evaluation of mitochondrial morphology, density, metabolic phenotype and mitochondrial oxygen consumption rate can be useful to unravel the deleterious mechanisms of HMW-AGEs. The link between oxidative stress produced by mitochondrial ROS production and contractile dysfunction has to be further investigated.

Finally, the chemical structure of our HMW-AGEs sample needs to be identified. Until now, established methods to identify AGEs are lacking, because of the diversity of the AGEs classes. However, better knowledge of the structure and composition of our HMW-AGEs sample is needed and requires further investigation (81).

5. Conclusion

Most studies investigate the effects of AGEs in a setting of diabetes or other diseases. To make conclusions about the role of AGEs in pathologies, generally an AGE inhibitor or breaker is added. On the other hand, studies apply AGEs to different types of cells in an acute setting. Freshly isolated cells or cell lines are only exposed to AGEs for a few hours. Next, a lot of studies only focus on AGEs with a LMW. Examining only LMW-AGEs might not be the best marker to evaluate the effect of AGEs in pathological situations because we know now that HMW-AGEs have an important role in cardiac dysfunction. This study is actually the first to examine the effect of HMW-AGEs on global cardiac function *in vivo* and cell function *in vitro* in a chronic setting independent of other diseases.

Our study show that rats subjected to high circulating HMW-AGEs display *in vitro* as well as *in vivo* structural and functional remodeling. Taken together, our data indicate that HMW-AGEs, an important component in our western diet, induce cardiac dysfunction. Changes observed at organ level are related to changes at the cellular level and altered excitation-contraction coupling. A better knowledge on the chemical nature of HMW-AGEs is required in order to be able to target them as therapeutic approaches in the future.

References

1. Ott C, Jacobs K, Haucke E, Navarrete Santos A, Grune T, Simm A. Role of advanced glycation end products in cellular signaling. Redox biology. 2014;2:411-29.
2. Singh R, Barden A, Mori T, Beilin L. Advanced glycation end-products: a review. Diabetologia. 2001;44(2):129-46.
3. Hegab Z, Gibbons S, Neyses L, Mamas MA. Role of advanced glycation end products in cardiovascular disease. World journal of cardiology. 2012;4(4):90-102.
4. Gkogkolou P, Bohm M. Advanced glycation end products: Key players in skin aging? Dermato-endocrinology. 2012;4(3):259-70.
5. Hartog JW, Voors AA, Bakker SJ, Smit AJ, van Veldhuisen DJ. Advanced glycation end-products (AGEs) and heart failure: pathophysiology and clinical implications. European journal of heart failure. 2007;9(12):1146-55.
6. Schalkwijk CG, Posthuma N, ten Brink HJ, ter Wee PM, Teerlink T. Induction of 1,2-dicarbonyl compounds, intermediates in the formation of advanced glycation end-products, during heat-sterilization of glucose-based peritoneal dialysis fluids. Peritoneal dialysis international : journal of the International Society for Peritoneal Dialysis. 1999;19(4):325-33.
7. Goldin A, Beckman JA, Schmidt AM, Creager MA. Advanced glycation end products: sparking the development of diabetic vascular injury. Circulation. 2006;114(6):597-605.
8. Lorenzi M. The polyol pathway as a mechanism for diabetic retinopathy: attractive, elusive, and resilient. Experimental diabetes research. 2007;2007:61038.
9. Wu J, Jin Z, Zheng H, Yan LJ. Sources and implications of NADH/NAD(+) redox imbalance in diabetes and its complications. Diabetes, metabolic syndrome and obesity : targets and therapy. 2016;9:145-53.
10. Miyata T, Wada Y, Cai Z, Iida Y, Horie K, Yasuda Y, et al. Implication of an increased oxidative stress in the formation of advanced glycation end products in patients with end-stage renal failure. Kidney international. 1997;51(4):1170-81.
11. Uribarri J, del Castillo MD, de la Maza MP, Filip R, Gugliucci A, Luevano-Contreras C, et al. Dietary advanced glycation end products and their role in health and disease. Advances in nutrition. 2015;6(4):461-73.
12. Clarke RE, Dordevic AL, Tan SM, Ryan L, Coughlan MT. Dietary Advanced Glycation End Products and Risk Factors for Chronic Disease: A Systematic Review of Randomised Controlled Trials. Nutrients. 2016;8(3):125.
13. Hellwig M, Geissler S, Matthes R, Peto A, Silow C, Brandsch M, et al. Transport of free and peptide-bound glycated amino acids: synthesis, transepithelial flux at Caco-2 cell monolayers, and interaction with apical membrane transport proteins. Chembiochem : a European journal of chemical biology. 2011;12(8):1270-9.
14. Koschinsky T, He CJ, Mitsuhashi T, Bucala R, Liu C, Buenting C, et al. Orally absorbed reactive glycation products (glycotoxins): an environmental risk factor in diabetic nephropathy. Proceedings of the National Academy of Sciences of the United States of America. 1997;94(12):6474-9.
15. Snedeker JG, Gautieri A. The role of collagen crosslinks in ageing and diabetes - the good, the bad, and the ugly. Muscles, ligaments and tendons journal. 2014;4(3):303-8.
16. Zieman S, Kass D. Advanced glycation end product cross-linking: pathophysiologic role and therapeutic target in cardiovascular disease. Congestive heart failure. 2004;10(3):144-9; quiz 50-1.
17. Bers DM. Cardiac excitation-contraction coupling. Nature. 2002;415(6868):198-205.
18. Fabiato A. Simulated calcium current can both cause calcium loading in and trigger calcium release from the sarcoplasmic reticulum of a skinned canine cardiac Purkinje cell. The Journal of general physiology. 1985;85(2):291-320.
19. Barry WH, Bridge JH. Intracellular calcium homeostasis in cardiac myocytes. Circulation. 1993;87(6):1806-15.

20. Bidasee KR, Nallani K, Yu Y, Cocklin RR, Zhang Y, Wang M, et al. Chronic diabetes increases advanced glycation end products on cardiac ryanodine receptors/calcium-release channels. Diabetes. 2003;52(7):1825-36.
21. Bidasee KR, Zhang Y, Shao CH, Wang M, Patel KP, Dincer UD, et al. Diabetes increases formation of advanced glycation end products on Sarco(endo)plasmic reticulum Ca2+-ATPase. Diabetes. 2004;53(2):463-73.
22. Litwinoff E, Hurtado Del Pozo C, Ramasamy R, Schmidt AM. Emerging Targets for Therapeutic Development in Diabetes and Its Complications: The RAGE Signaling Pathway. Clinical pharmacology and therapeutics. 2015;98(2):135-44.
23. Zhu H, Ding Q. Lower expression level of two RAGE alternative splicing isoforms in Alzheimer's disease. Neuroscience letters. 2015;597:66-70.
24. Sternberg Z, Chiotti A, Tario J, Chichelli T, Patel N, Chadha K, et al. Reduced expression of membrane-bound (m)RAGE is a biomarker of multiple sclerosis disease progression. Immunobiology. 2016;221(2):193-8.
25. Yang PS, Lee SH, Park J, Kim TH, Uhm JS, Joung B, et al. Atrial tissue expression of receptor for advanced glycation end-products (RAGE) and atrial fibrosis in patients with mitral valve disease. International journal of cardiology. 2016;220:1-6.
26. Cohen MM, Jr. Perspectives on RAGE signaling and its role in cardiovascular disease. American journal of medical genetics Part A. 2013;161A(11):2750-5.
27. Jules J, Maiguel D, Hudson BI. Alternative splicing of the RAGE cytoplasmic domain regulates cell signaling and function. PloS one. 2013;8(11):e78267.
28. Sarkany Z, Ikonen TP, Ferreira-da-Silva F, Saraiva MJ, Svergun D, Damas AM. Solution structure of the soluble receptor for advanced glycation end products (sRAGE). The Journal of biological chemistry. 2011;286(43):37525-34.
29. Sterenczak KA, Willenbrock S, Barann M, Klemke M, Soller JT, Eberle N, et al. Cloning, characterisation, and comparative quantitative expression analyses of receptor for advanced glycation end products (RAGE) transcript forms. Gene. 2009;434(1-2):35-42.
30. Xie J, Mendez JD, Mendez-Valenzuela V, Aguilar-Hernandez MM. Cellular signalling of the receptor for advanced glycation end products (RAGE). Cellular signalling. 2013;25(11):2185-97.
31. Shang L, Ananthakrishnan R, Li Q, Quadri N, Abdillahi M, Zhu Z, et al. RAGE modulates hypoxia/reoxygenation injury in adult murine cardiomyocytes via JNK and GSK-3beta signaling pathways. PloS one. 2010;5(4):e10092.
32. Ramasamy R, Schmidt AM. Receptor for advanced glycation end products (RAGE) and implications for the pathophysiology of heart failure. Current heart failure reports. 2012;9(2):107-16.
33. Gerdemann A, Lemke HD, Nothdurft A, Heidland A, Munch G, Bahner U, et al. Low-molecular but not high-molecular advanced glycation end products (AGEs) are removed by high-flux dialysis. Clinical nephrology. 2000;54(4):276-83.
34. Miura J, Yamagishi S, Uchigata Y, Takeuchi M, Yamamoto H, Makita Z, et al. Serum levels of non-carboxymethyllysine advanced glycation endproducts are correlated to severity of microvascular complications in patients with Type 1 diabetes. Journal of diabetes and its complications. 2003;17(1):16-21.
35. Poulsen MW, Andersen JM, Hedegaard RV, Madsen AN, Krath BN, Monosik R, et al. Short-term effects of dietary advanced glycation end products in rats. The British journal of nutrition. 2016;115(4):629-36.
36. Bucciarelli LG, Kaneko M, Ananthakrishnan R, Harja E, Lee LK, Hwang YC, et al. Receptor for advanced-glycation end products: key modulator of myocardial ischemic injury. Circulation. 2006;113(9):1226-34.
37. Deluyker D, Ferferieva V, Noben JP, Swennen Q, Bronckaers A, Lambrichts I, et al. Cross-linking versus RAGE: How do high molecular weight advanced glycation products induce cardiac dysfunction? International journal of cardiology. 2016;210:100-8.

38. Heidland A, Sebekova K, Frangiosa A, De Santo LS, Cirillo M, Rossi F, et al. Paradox of circulating advanced glycation end product concentrations in patients with congestive heart failure and after heart transplantation. Heart. 2004;90(11):1269-74.
39. Penfold SA, Coughlan MT, Patel SK, Srivastava PM, Sourris KC, Steer D, et al. Circulating high-molecular-weight RAGE ligands activate pathways implicated in the development of diabetic nephropathy. Kidney international. 2010;78(3):287-95.
40. Nishizawa Y, Wada R, Baba M, Takeuchi M, Hanyu-Itabashi C, Yagihashi S. Neuropathy induced by exogenously administered advanced glycation end-products in rats. Journal of diabetes investigation. 2010;1(1-2):40-9.
41. Coughlan MT, Yap FY, Tong DC, Andrikopoulos S, Gasser A, Thallas-Bonke V, et al. Advanced glycation end products are direct modulators of beta-cell function. Diabetes. 2011;60(10):2523-32.
42. Vlassara H, Fuh H, Makita Z, Krungkrai S, Cerami A, Bucala R. Exogenous advanced glycosylation end products induce complex vascular dysfunction in normal animals: a model for diabetic and aging complications. Proceedings of the National Academy of Sciences of the United States of America. 1992;89(24):12043-7.
43. Darbandi Azar A, Tavakoli F, Moladoust H, Zare A, Sadeghpour A. Echocardiographic evaluation of cardiac function in ischemic rats: value of m-mode echocardiography. Research in cardiovascular medicine. 2014;3(4):e22941.
44. Candido R, Forbes JM, Thomas MC, Thallas V, Dean RG, Burns WC, et al. A breaker of advanced glycation end products attenuates diabetes-induced myocardial structural changes. Circulation research. 2003;92(7):785-92.
45. Herrmann KL, McCulloch AD, Omens JH. Glycated collagen cross-linking alters cardiac mechanics in volume-overload hypertrophy. American journal of physiology Heart and circulatory physiology. 2003;284(4):H1277-84.
46. Buchanan LV, Warner WA, Arthur SR, Gleason CR, Lewen G, Levesque PC, et al. Evaluation of cardiac function in unrestrained dogs and monkeys using left ventricular dP/dt. Journal of pharmacological and toxicological methods. 2016;80:51-8.
47. Cheng G, Wang LL, Qu WS, Long L, Cui H, Liu HY, et al. C16, a novel advanced glycation endproduct breaker, restores cardiovascular dysfunction in experimental diabetic rats. Acta pharmacologica Sinica. 2005;26(12):1460-6.
48. Liu J, Masurekar MR, Vatner DE, Jyothirmayi GN, Regan TJ, Vatner SF, et al. Glycation end-product cross-link breaker reduces collagen and improves cardiac function in aging diabetic heart. American journal of physiology Heart and circulatory physiology. 2003;285(6):H2587-91.
49. Ko SY, Lin IH, Shieh TM, Ko HA, Chen HI, Chi TC, et al. Cell hypertrophy and MEK/ERK phosphorylation are regulated by glyceraldehyde-derived AGEs in cardiomyocyte H9c2 cells. Cell biochemistry and biophysics. 2013;66(3):537-44.
50. Watkins SJ, Borthwick GM, Arthur HM. The H9C2 cell line and primary neonatal cardiomyocyte cells show similar hypertrophic responses in vitro. In vitro cellular & developmental biology Animal. 2011;47(2):125-31.
51. Peter AK, Bjerke MA, Leinwand LA. Biology of the cardiac myocyte in heart disease. Molecular biology of the cell. 2016;27(14):2149-60.
52. Tikellis C, Thomas MC, Harcourt BE, Coughlan MT, Pete J, Bialkowski K, et al. Cardiac inflammation associated with a Western diet is mediated via activation of RAGE by AGEs. American journal of physiology Endocrinology and metabolism. 2008;295(2):E323-30.
53. Ma H, Li SY, Xu P, Babcock SA, Dolence EK, Brownlee M, et al. Advanced glycation endproduct (AGE) accumulation and AGE receptor (RAGE) up-regulation contribute to the onset of diabetic cardiomyopathy. Journal of cellular and molecular medicine. 2009;13(8B):1751-64.
54. Ceylan-Isik AF, Wu S, Li Q, Li SY, Ren J. High-dose benfotiamine rescues cardiomyocyte contractile dysfunction in streptozotocin-induced diabetes mellitus. Journal of applied physiology. 2006;100(1):150-6.

55. Ginsburg KS, Bers DM. Modulation of excitation-contraction coupling by isoproterenol in cardiomyocytes with controlled SR Ca2+ load and Ca2+ current trigger. The Journal of physiology. 2004;556(Pt 2):463-80.
56. Robinet A, Alouane L, Hoizey G, Millart H. Advanced-glycation end products (AGEs) derived from glycated albumin suppress early beta1-adrenergic preconditioning. Fundamental & clinical pharmacology. 2007;21(1):35-43.
57. Piacentino V, 3rd, Weber CR, Chen X, Weisser-Thomas J, Margulies KB, Bers DM, et al. Cellular basis of abnormal calcium transients of failing human ventricular myocytes. Circulation research. 2003;92(6):651-8.
58. Bracken N, Howarth FC, Singh J. Effects of streptozotocin-induced diabetes on contraction and calcium transport in rat ventricular cardiomyocytes. Annals of the New York Academy of Sciences. 2006;1084:208-22.
59. Bracken NK, Woodall AJ, Howarth FC, Singh J. Voltage-dependence of contraction in streptozotocin-induced diabetic myocytes. Molecular and cellular biochemistry. 2004;261(1-2):235-43.
60. Lu Z, Ballou LM, Jiang YP, Cohen IS, Lin RZ. Restoration of defective L-type Ca2+ current in cardiac myocytes of type 2 diabetic db/db mice by Akt and PKC-iota. Journal of cardiovascular pharmacology. 2011;58(4):439-45.
61. Pereira L, Matthes J, Schuster I, Valdivia HH, Herzig S, Richard S, et al. Mechanisms of [Ca2+]i transient decrease in cardiomyopathy of db/db type 2 diabetic mice. Diabetes. 2006;55(3):608-15.
62. Yuill KH, Al Kury LT, Howarth FC. Characterization of L-type calcium channel activity in atrioventricular nodal myocytes from rats with streptozotocin-induced Diabetes mellitus. Physiological reports. 2015;3(11).
63. Bito V, Heinzel FR, Biesmans L, Antoons G, Sipido KR. Crosstalk between L-type Ca2+ channels and the sarcoplasmic reticulum: alterations during cardiac remodelling. Cardiovascular research. 2008;77(2):315-24.
64. Bers DM, Despa S. Cardiac myocytes Ca2+ and Na+ regulation in normal and failing hearts. Journal of pharmacological sciences. 2006;100(5):315-22.
65. Bers DM. Altered cardiac myocyte Ca regulation in heart failure. Physiology. 2006;21:380-7.
66. Zarain-Herzberg A, Garcia-Rivas G, Estrada-Aviles R. Regulation of SERCA pumps expression in diabetes. Cell calcium. 2014;56(5):302-10.
67. Zhao XY, Hu SJ, Li J, Mou Y, Chen BP, Xia Q. Decreased cardiac sarcoplasmic reticulum Ca2+ -ATPase activity contributes to cardiac dysfunction in streptozotocin-induced diabetic rats. Journal of physiology and biochemistry. 2006;62(1):1-8.
68. Kim HW, Ch YS, Lee HR, Park SY, Kim YH. Diabetic alterations in cardiac sarcoplasmic reticulum Ca2+-ATPase and phospholamban protein expression. Life sciences. 2001;70(4):367-79.
69. Teshima Y, Takahashi N, Saikawa T, Hara M, Yasunaga S, Hidaka S, et al. Diminished expression of sarcoplasmic reticulum Ca(2+)-ATPase and ryanodine sensitive Ca(2+)Channel mRNA in streptozotocin-induced diabetic rat heart. Journal of molecular and cellular cardiology. 2000;32(4):655-64.
70. Petrova R, Yamamoto Y, Muraki K, Yonekura H, Sakurai S, Watanabe T, et al. Advanced glycation endproduct-induced calcium handling impairment in mouse cardiac myocytes. Journal of molecular and cellular cardiology. 2002;34(10):1425-31.
71. Ren J, Gintant GA, Miller RE, Davidoff AJ. High extracellular glucose impairs cardiac E-C coupling in a glycosylation-dependent manner. The American journal of physiology. 1997;273(6 Pt 2):H2876-83.
72. Magyar J, Rusznak Z, Szentesi P, Szucs G, Kovacs L. Action potentials and potassium currents in rat ventricular muscle during experimental diabetes. Journal of molecular and cellular cardiology. 1992;24(8):841-53.
73. Ide T, Tsutsui H, Hayashidani S, Kang D, Suematsu N, Nakamura K, et al. Mitochondrial DNA damage and dysfunction associated with oxidative stress in failing hearts after myocardial infarction. Circulation research. 2001;88(5):529-35.

74. Wilding JR, Joubert F, de Araujo C, Fortin D, Novotova M, Veksler V, et al. Altered energy transfer from mitochondria to sarcoplasmic reticulum after cytoarchitectural perturbations in mice hearts. The Journal of physiology. 2006;575(Pt 1):191-200.
75. Kayama Y, Raaz U, Jagger A, Adam M, Schellinger IN, Sakamoto M, et al. Diabetic Cardiovascular Disease Induced by Oxidative Stress. International journal of molecular sciences. 2015;16(10):25234-63.
76. Hafstad AD, Nabeebaccus AA, Shah AM. Novel aspects of ROS signalling in heart failure. Basic research in cardiology. 2013;108(4):359.
77. Kranstuber AL, Del Rio C, Biesiadecki BJ, Hamlin RL, Ottobre J, Gyorke S, et al. Advanced glycation end product cross-link breaker attenuates diabetes-induced cardiac dysfunction by improving sarcoplasmic reticulum calcium handling. Frontiers in physiology. 2012;3:292.
78. Hofmann PA, Menon V, Gannaway KF. Effects of diabetes on isometric tension as a function of [Ca2+] and pH in rat skinned cardiac myocytes. The American journal of physiology. 1995;269(5 Pt 2):H1656-63.
79. Akella AB, Ding XL, Cheng R, Gulati J. Diminished Ca2+ sensitivity of skinned cardiac muscle contractility coincident with troponin T-band shifts in the diabetic rat. Circulation research. 1995;76(4):600-6.
80. Ward ML, Crossman DJ. Mechanisms underlying the impaired contractility of diabetic cardiomyopathy. World journal of cardiology. 2014;6(7):577-84.
81. Takeuchi M, Takino J, Furuno S, Shirai H, Kawakami M, Muramatsu M, et al. Assessment of the concentrations of various advanced glycation end-products in beverages and foods that are commonly consumed in Japan. PloS one. 2015;10(3):e0118652.

Curriculum Vitae

Skills

Competencies:

Enthusiastic, dedicated, motivated and hard-working, well-organized, works well under pressure, independent – team player, responsible, punctual, flexible

Laboratory techniques:

Left ventricular pressure measurements in rats, echocardiographic measurements in rats, cardiomyocyte isolation, patch clamp, unloaded cell shortening measurements, protein expression measurements, immunohistochemistry, ELISA, microscopy

Working experience during Internships

Master research project (Senior practical training)

"High molecular weight Advanced Glycated End Products cause reduced and slower cell shortening by decreasing I_{CaL}.". Biomedical Research Institute (Biomed) department Cardiology, Physiology, Hasselt University. Supervisor: Prof. Dr. V. Bito

Publications:

D. Deluyker, L. Evens, V. Bito. (2017). Advanced glycation end products (AGEs) and cardiovascular dysfunction: focus on high molecular weight AGEs. Submitted to Amino Acids.

Abstracts:

D. Deluyker, L. Evens, M. Verboven, V. Bito. (2017). Glycated proteins in cardiac dysfunction: Big molecules, Huge impact. Submitted to American Heart Associaton.

Master research project (Junior practical training)

"Evaluation of heart, kidney and liver damage in a rat model for cardiorenal syndrome". Biomedical Research Institute (Biomed) department Cardiology, Physiology, Hasselt University. Supervisor: Prof. Dr. Q. Swennen

Bachelor research project

"Verandering van expressie van SERCA, PLN en NCX in een ratmodel met hartfalen". Biomedical Research Institute (Biomed) department Cardiology, Physiology, Hasselt University. Supervisor: Prof. Dr. V. Bito

Education

- Master Clinical and Molecular Sciences
  2015 – 2017
  Hasselt University
    Additional courses during first Master year:
      - Laboratory animal sciences: FELASA C certificate
      - Cardiology

- Bachelor Biomedical Sciences
  2012 – 2015
  Hasselt University

Auteursrechtelijke overeenkomst

Ik/wij verlenen het wereldwijde auteursrecht voor de ingediende eindverhandeling:
High molecular weight Advanced Glycated End Products cause reduced and slower cell shortening by decreasing I_{CaL}

Richting: **master in de biomedische wetenschappen-klinische moleculaire wetenschappen**
Jaar: **2017**

in alle mogelijke mediaformaten, - bestaande en in de toekomst te ontwikkelen - , aan de Universiteit Hasselt.

Niet tegenstaand deze toekenning van het auteursrecht aan de Universiteit Hasselt behoud ik als auteur het recht om de eindverhandeling, - in zijn geheel of gedeeltelijk -, vrij te reproduceren, (her)publiceren of distribueren zonder de toelating te moeten verkrijgen van de Universiteit Hasselt.

Ik bevestig dat de eindverhandeling mijn origineel werk is, en dat ik het recht heb om de rechten te verlenen die in deze overeenkomst worden beschreven. Ik verklaar tevens dat de eindverhandeling, naar mijn weten, het auteursrecht van anderen niet overtreedt.

Ik verklaar tevens dat ik voor het materiaal in de eindverhandeling dat beschermd wordt door het auteursrecht, de nodige toelatingen heb verkregen zodat ik deze ook aan de Universiteit Hasselt kan overdragen en dat dit duidelijk in de tekst en inhoud van de eindverhandeling werd genotificeerd.

Universiteit Hasselt zal mij als auteur(s) van de eindverhandeling identificeren en zal geen wijzigingen aanbrengen aan de eindverhandeling, uitgezonderd deze toegelaten door deze overeenkomst.

Voor akkoord,

Evens, Lize

Datum: **8/06/2017**